Atmospheric Response to North Pacific SST: The Role of Ocean–Atmosphere Coupling*

ZHENGYU LIU AND LIXIN WU

Center for Climatic Research, University of Wisconsin—Madison, Madison, Wisconsin

(Manuscript received 2 October 2003, in final form 11 December 2003)

ABSTRACT

Atmospheric response to a midlatitude winter SST anomaly is studied in a coupled ocean–atmosphere general circulation model. The role of ocean–atmosphere coupling is examined with ensemble experiments of different coupling configurations. The atmospheric response is found to depend critically on ocean–atmosphere coupling. The full coupling experiment produces the strongest warm-ridge response and agrees the best with a statistical estimation of the atmospheric response. The fixed SST experiment and the thermodynamic coupling experiment also generate a warm-ridge response, but with a substantially weaker magnitude. This weaker warm-ridge response is associated with an excessive heat flux into the atmosphere, which tends to force an anomalous warm-low response and, therefore, weakens the warm-ridge response of the full coupling experiment.

This study suggests that the atmospheric response is associated with both the SST and heat flux. The SST forcing favors a warm-ridge response, while the heat flux forcing tends to be associated with a warm-low response. The correct atmospheric response is generated in the fully coupled model that produces the correct combination of SST and heat flux naturally.

1. Introduction

The response of the atmosphere to midlatitude SST variability remains as one major challenge for our understanding of extratropical climate variability. In contrast to the tropical atmosphere, which has a largely linear stationary response to SST, the extratropical atmosphere has a much more complicated response because of the strong atmospheric internal variability. Most previous studies have investigated the atmospheric response to a prescribed SST anomaly in atmospheric general circulation models (AGCMs) (Palmer and Sun 1985; Pitcher et al. 1988; Kushnir and Lau 1992; Ferranti et al. 1994; Peng et al. 1995, 1997; Kushnir and Held 1996; Latif and Barnett 1994, 1996). This approach, called the Atmospheric Model Intercomparison Project (AMIP) approach, has produced widely different results (see the review by Kushnir et al. 2002). Some produce a linear baroclinic response with a surface low pressure downstream of a warm SST anomaly, while some others produce an equivalent barotropic high response downstream of a warm SST anomaly (warm-ridge response); some experiments show strongly nonlinear dependence of the response; some experiments are sensitive to the seasonality, and even the sign, of the SST anomaly. In spite of the diverse results, most recent AMIP studies recognized that the atmospheric response to midlatitude SST is not as predicted in linear theories (Hoskins and Karoly 1981). In particular, it is recognized that nonlinear feedback of atmospheric transient eddies plays a critical role in the warm-ridge response (Peng et al. 1995, 1997; Peng and Whitaker 1999; Peng and Robinson 2001).

Recently, it has been pointed out that the AGCM response also depends on the forcing condition at the lower boundary (Barsugli and Battisti 1998; Bretherton and Battisti 2000). Two recent attempts used a coupled AGCM–slab ocean model, in which an anomalous surface heat flux is prescribed to force the atmosphere (Yulaeva et al. 2001; Sutton and Mathieu 2002). In both studies, the heat flux forces a low pressure downstream (warm-low response). This naturally raises the question: Which type of experiments, fixed SST or fixed flux, is more correct? Regardless of the answer to this question, the dramatic difference of the atmospheric responses in these two types of experiments suggests that the response of the atmosphere depends not only on its dynamics but also on its coupling with the ocean. This has motivated us here to further study the atmospheric response to a midlatitude SST anomaly, with the focus on the role of ocean–atmosphere coupling.

A fully coupled ocean–atmosphere general circulation model is used to study the atmospheric response to

* Center for Climatic Research, University of Wisconsin—Madison Contribution Number 838.

Corresponding author address: Z. Liu, Center for Climatic Research, 1225 W. Dayton St., Madison, WI 53706.
E-mail: zliu3@wisc.edu

a North Pacific December SST anomaly. To understand the role of ocean–atmosphere coupling, four sets of ensemble experiments are performed with different coupling configurations: the fixed SST ensemble (AMIP), the fully coupled ensemble, the thermodynamically coupled ensemble, and the fixed heat flux ensemble. The atmospheric responses of these ensemble experiments are compared with a statistical estimate of the atmospheric response. The AMIP generates a weak warm-ridge response, consistent with most previous high-resolution AGCM experiments. A similar response is produced in the thermodynamically coupled ensemble in which the dynamic coupling associated with the Ekman advection is eliminated. In contrast, the atmosphere in the fully coupled ensemble exhibits a strong warm-ridge response with a magnitude that is consistent with the statistical estimate. The different amplitude of atmospheric response between the fully coupled ensemble and other ensembles is found to be accompanied by different heat flux forcing to the atmosphere. While the fully coupled ensemble only has a weak heat flux forcing to the atmosphere, the AMIP ensemble and thermodynamically coupled ensemble have an excessive heat flux forcing. This excessive heat flux tends to generate a warm-low atmospheric response, as suggested by the fixed flux ensemble and previous works (Yulaeva et al. 2001; Sutton and Mathieu 2002), which in turn weakens the warm-ridge response in the fully coupled ensemble and therefore results in a weak warm-ridge response. Our study therefore suggests that the atmospheric response depends critically not only on the SST forcing but also on the heat flux forcing. The correct response is achieved in neither the AMIP ensemble nor the flux-forced ensemble (FXE), but is achieved in the fully coupled ensemble in which the correct combination of SST and heat flux is generated naturally.

This paper is arranged as follows. Section 2 compares the model North Pacific climate variability with the observation. Section 3 studies the atmospheric response in AMIP. Section 4 investigates the effect of ocean–atmosphere coupling on atmospheric responses in the fully coupled ensemble, while section 5 further studies the roles of thermodynamic coupling and dynamic coupling. Section 6 investigates both the atmospheric forcing and atmospheric response and the implied ocean–atmosphere feedback. A summary and further discussions are given in section 7.

2. Model and observation

We used the Fast Ocean Atmosphere Model (FOAM) (Jacob 1997). FOAM is a fully coupled ocean–atmosphere general circulation model without flux adjustment. The atmospheric component of FOAM is a fully parallel version of the National Center for Atmospheric Research (NCAR) community climate model, version 2 (CCM2), in which the atmospheric physics are replaced by those of NCAR CCM3. We used version 1.5 of FOAM (FOAM 1.5). The atmosphere has a R15 resolution (equivalent grid spacing about 4.5° lat × 7.5° lon), with 18 vertical levels. The ocean component is a *z* coordinate model, much like the Los Alamos National Laboratory (LANL) Parallel Ocean Program (POP), with a resolution of 1.4° latitude × 2.8° longitude × 24 level. The coupled FOAM is integrated for 1000 years with the last 400 years being used as our control simulation (CTRL).

FOAM1.5 has a similar performance to the previous FOAM1.0. The performance of FOAM1.0 has been documented extensively, including its model climatology (Jacob 1997; Liu et al. 2003) and Pacific climate variability (Liu et al. 2000, 2002; Wu et al. 2003; Wu and Liu 2003). Overall, FOAM captures most major features of the observed climatology as in most state-of-the-art climate models, such as the NCAR Climate System Model (CSM) (Boville and Gent 1998; Otto-Bliesner and Brady 2001). FOAM also produces a reasonable ENSO, albeit with a somewhat smaller variance than the observation.

FOAM simulates a reasonable North Pacific climate variability (Wu et al. 2003; Wu and Liu 2003). Here, we will focus on the atmospheric response to SST variability in the western North Pacific of the Kuroshio extension region (defined as 35°–45°N, 140°E–180° here). We will analyze the CTRL simulation, as well as the National Centers for Environmental Prediction (NCEP)–NCAR reanalysis, the latter being used as the proxy for observation. The rest of the section serves two purposes. First, we want to compare the model North Pacific climate variability with the observation. Second, we want to provide a benchmark of model atmospheric response to be compared with later ensemble experiments.

Seasonal dependence of ocean–atmosphere interaction in the Kuroshio Extension region can be inferred from the lagged correlation between regional SST and the overlying atmospheric sea level pressure (SLP) and wind. For the SST of a particular calendar month, both the NCEP–NCAR reanalysis (Fig. 1a) and CTRL (Fig. 1b) show a strong asymmetry with lag, with a higher correlation at negative lags (atmosphere leads). This asymmetric correlation suggests that midlatitude monthly SST variability is forced predominantly by the atmosphere (Frankignoul and Hasselmann 1977; Frankignoul et al. 1998). In both the observation and model, the atmosphere tends to force a warmer SST with a higher SLP and weaker westerly wind, as seen in the positive correlation between SLP and SST and the negative correlation between zonal wind and SST at lag −1 month (Figs. 1a,b).

The correlation is weak at positive lags (SST leads). This weak correlation, nevertheless, implies a possible atmospheric response to SST. The atmospheric response has a strong seasonal dependence, with the strongest response occurring later in the calendar year, as seen in the significant correlation at positive lags (October–De-

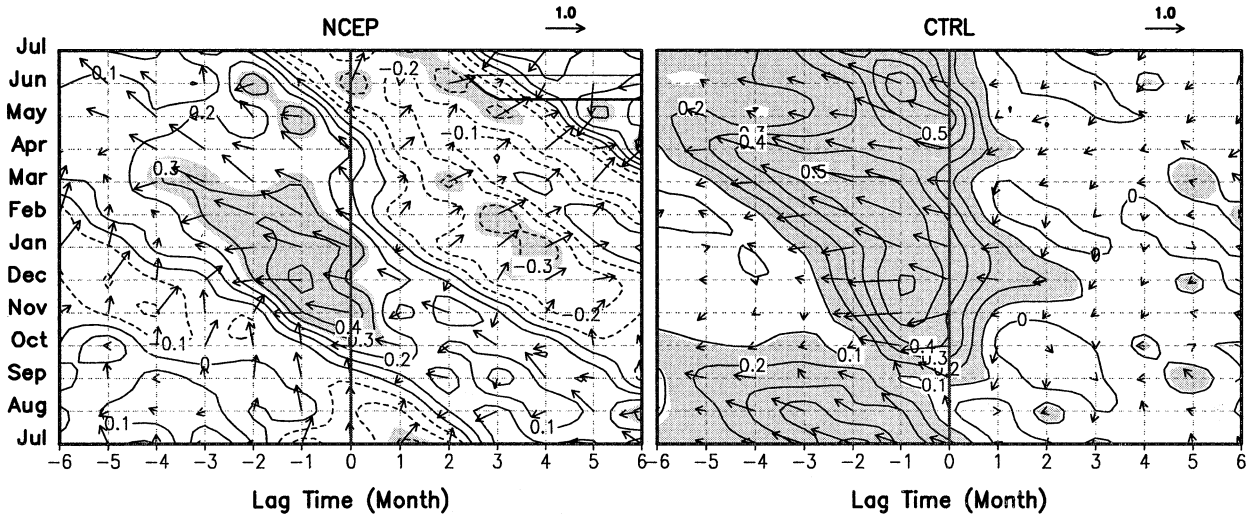

FIG. 1. Lagged correlation between the western North Pacific SST and the atmosphere surface wind (vector) and sea level pressure (contour) for different calendar months. All variables are averaged in the Kuroshio Extension region (35°–45°N, 140°E–180°). Positive lags indicate SST lead of atmosphere and negative lags atmosphere lead of SST: (a) NCEP–NCAR reanalysis and (b) CTRL simulation. Contour interval is 0.1 hPa K^{-1} for SLP and the vector unit is 1 m s^{-1} K^{-1}. Negative values are dashed. Shading indicates the correlation statistically different from zero at the 95% level.

cember in the NCEP–NCAR reanalysis and mainly December in the model, at lags +1 and +2 in Figs. 1a and 1b). This seasonal dependence of the atmospheric response has been discussed in AGCMs (Peng et al. 1995) and in the observed North Atlantic (Cajza and Frankignoul 2002). The model (Fig. 1b) fails to produce the substantial correlation at long SST leads (+3 to +6 month) from late summer to fall in the NCEP–NCAR reanalysis (Fig. 1a). This large correlation at long SST leads is associated with the long persistence time of SST, which in turn is related to the reemergence mechanism (Alexander et al. 1999). The absence of this long lead correlation in the model appears to be caused by a shallower winter mixed layer in the model western North Pacific, which results in shorter SST persistence (not shown) and, in turn, a weaker atmospheric response to SST.

In estimating the atmospheric response to midlatitude SST, it is essential to filter out the noise associated with atmospheric internal variability. Frankignoul et al. (1998) proposed that the atmospheric response to midlatitude SST variability should be estimated with the aid of the SST-lead covariance rather than with the instantaneous covariance alone (also see Cajza and Frankignoul 2002). Following this approach, we assume a linear relation, $A(t) = \lambda_A T(t) + N(t)$, between an atmosphere variable A and SST anomaly T. Here N is a random noise due to the atmospheric internal variability and $\lambda_A T(t)$ represents the part of atmospheric response at month t to the SST anomaly at the same month t (with a short atmospheric response time neglected). The response parameter λ_A is estimated as

$$\lambda_A = \langle T(t - \tau), A(t)\rangle / \langle T(t - \tau), T(t)\rangle, \qquad (1)$$

where angle brackets represent the cross-covariance and the SST-lead time $\tau > 0$ should be longer than the decorrelation time of the atmospheric internal variability N. With the monthly data here, $\tau = 1$ month is used as in Frankignoul et al. (1998).

The pattern of the December atmospheric response to December SST is estimated statistically using (1) with T being the SST averaged in the Kuroshio Extension region and A being an atmospheric variable at each grid point. Both the NCEP–NCAR reanalysis (Fig. 2) and model (Fig. 3) show a dominant equivalent barotropic high over the Aleutian low and an accompanying surface easterly in mid latitudes. The magnitude of the model atmospheric response, however, is weaker than the observation by 30%. The North Pacific high pressure anomaly is shifted southward by 10° in the model relative to the reanalysis. Overall, nevertheless, our model captures the major features of the observed atmospheric response and therefore should be relevant to the real world.

The statistical estimate here should be treated with caution because of limitations of the method. The climate model, however, provides an alternative to understand the atmospheric response dynamically. This dynamic assessment of the atmospheric response can be accomplished using specifically designed sensitivity experiments as discussed in the following sections.

3. AMIP response

The traditional AMIP experiment provides not only a reference for coupled experiments in later sections but also a calibration for our AGCM against other AGCMs.

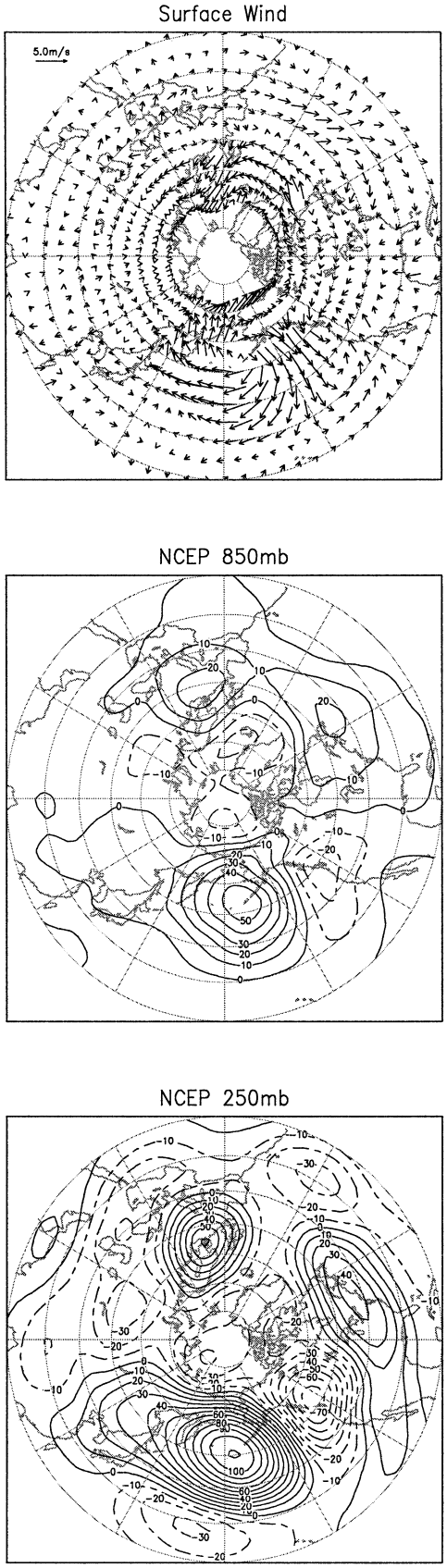

A 40-member AMIP ensemble is generated as follows. First, a 400-yr control simulation (CTRL-AMIP) is performed using a partial coupling strategy in FOAM such that the atmosphere is forced by a prescribed seasonal cycle of global SST (while the ocean is forced by the flux calculated from the atmosphere and the predicted SST, see Wu et al. 2003). The prescribed SST seasonal cycle is derived from the climatology of the fully coupled CTRL simulation. Second, a bell-shaped warm SST anomaly is added to the prescribed SST seasonal cycle in the Kuroshio Extension region (Fig. 4) as the anomalous forcing to the atmosphere. The SST anomaly has a maximum of 2 K and an area average of 1.2 K in the Kuroshio Extension. Each ensemble member is integrated for two months starting from a 1 November atmosphere state selected from the CTRL-AMIP every 8 years apart. The December climate anomaly is the difference between the December climate of each ensemble member and the corresponding part of the CTRL-AMIP.

The ensemble mean December atmospheric response exhibits a statistically significant warm-ridge response with a downstream equivalent barotropic high over the subpolar North Pacific (Figs. 5c,d), a midlatitude surface easterly over the Kuroshio Extension region (Fig. 5a), a positive (upward) turbulent heat flux and increased precipitation above the SST anomaly, and a negative surface heat flux and decreased precipitation downstream (Figs. 5a,b). (The significance test in this paper is based on the Student's *t* test with each ensemble member treated as being independent.) The pattern of the AMIP atmospheric response resembles the statistical estimation (Fig. 3). However, the magnitude of the AMIP response is much weaker. The height response on the 250- and 850-hPa isobars are over 70 and 30 m in the statistical estimation, but only about 40 and 20 m in AMIP. Notice that for a fair comparison between Figs. 3 and 5, the atmospheric response in the latter should be divided by a factor of 1.2 because the AMIP SST anomaly averaged in the Kuroshio Extension region is 1.2°C in Fig. 5, while Fig. 3 is for the atmospheric response per 1°C SST variability in the Kuroshio Extension region. Taking this correction into account, the AMIP atmospheric response is about half that of the statistical estimation.

The vertical structure of the AMIP response along 40°N shows an equivalent barotropic high centered downstream of the SST anomaly (Fig. 6a1). The warm temperature anomaly has two centers: a shallow center locally over the SST anomaly and a midair center downstream of the SST anomaly (Fig. 6a2). The shallow

←

FIG. 2. Statistical estimation of the atmospheric response to the Kuroshio Extension SST variability using Eq. (1) for the NCEP–NCAR reanalysis. (a) Surface wind (m s^{-1} K^{-1}), (b) 850-hPa, and (c) 250-hPa geopotential height (contour interval 10 m K^{-1}). Negative contours are dashed.

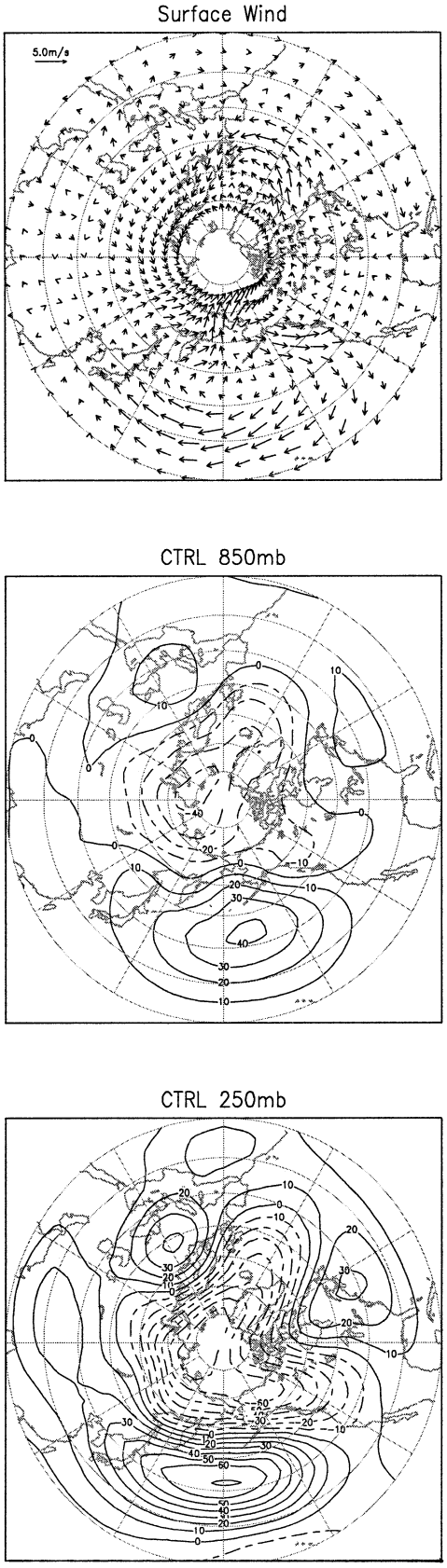

FIG. 3. As in Fig. 2 but for the CTRL simulation.

warm temperature center appears to be forced directly by the diabatic heating, which also exhibits a shallow positive center locally above the SST anomaly (Fig. 6a3). This shallow diabatic heating center is associated with an increased latent heating, ascending motion, and precipitation (not shown). The midair center of warm temperature, however, is not caused by diabatic heating because diabatic heating exhibits a broad midair cooling center there (Fig. 6a3), which is associated with an anomalous descending and precipitation reduction (not shown). Instead, the midair warming appears to be caused by the warm adiabatic warming associated with the descending motion (see later Fig. A1a3). These features discussed above are consistent with Peng et al. (1997, the February case). Further analyses of the thermodynamic and vorticity budgets also show strong similarity with Peng et al. (1997) (see appendix A). The overall resemblance with Peng et al. (1997) suggests that FOAM and Peng's model may share common mechanisms for the warm-ridge response, as elucidated by Peng and Whitaker (1999) and Peng and Robinson (2001).

The warm-ridge response in our AMIP is somewhat unexpected, given that this response has not been produced in any published low-resolution (R15) AMIP experiment (Pitcher et al. 1988; Kushnir and Lau 1992; Kushnir and Held 1996; see Kushnir et al. 2002 for a review). In the mean time, our AMIP response agrees well with most high-resolution AMIP experiments in either the North Pacific (Ferranti et al. 1994; the February case of Peng et al. 1997; Latif and Barnett 1994) or the North Atlantic (Palmer and Sun 1985; Peng et al. 1995). It is unclear why our R15 AMIP response is different from other R15 AMIP experiments. Since the upper-level eddy vorticity forcing is believed to be critical for the warm-ridge response and since there is evidence suggesting that the transient eddy flux forcing is not well simulated in some low-resolution models (W. Robinson 2003, personal communication), one may question the nature of the warm-ridge response in FOAM. Classical linear theories suggest that, although the linear atmospheric response in most cases are linearly baroclinic, there are special circumstances when a linear atmosphere model can produce a warm-ridge response (Frankignoul 1985; Palmer and Sun 1985; W. Robinson 2003, personal communication). We believe, however, that the warm-ridge response in FOAM is not dominated by the linear response. Partly, our belief is based on the thermodynamic and vorticity budget analyses using the monthly output (appendix A). These analyses show a strong resemblance to those in the high-resolution model of Peng et al. (1997). We have further performed the column (850–250 hPa) averaged vorticity budget (not shown) and found that the ridge response is forced overwhelmingly by a negative residual vorticity forcing, which should be dominated by the eddy flux forcing. For a more definite conclusion, we well need to use daily outputs that resolve the transient eddies

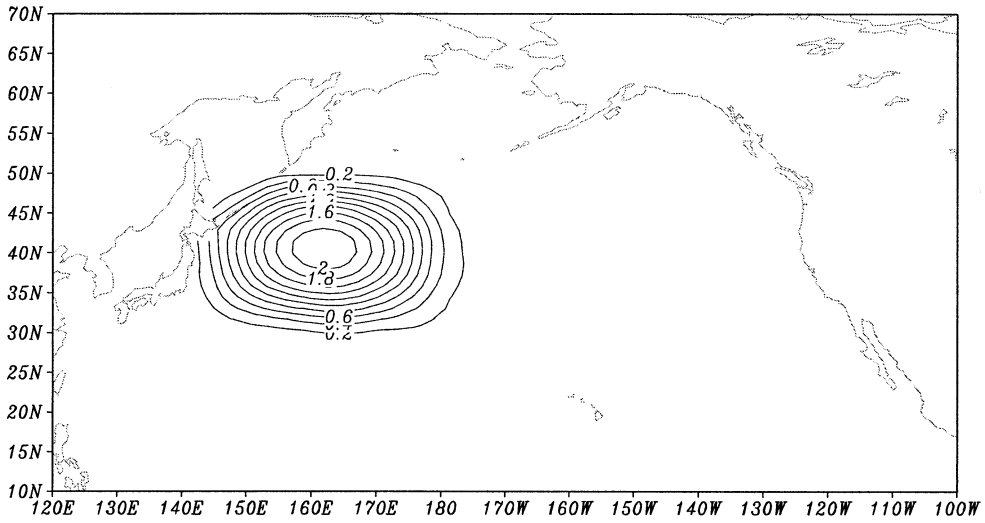

FIG. 4. The SST anomaly used to force the atmosphere in AMIP.

explicitly. Unfortunately, all of our model outputs are in monthly averages and, therefore, we have to defer the eddy-forcing study for future work. Accidentally, we notice that FOAM has 18 levels, while all published R15 AMIP experiments have only 9 levels (Pitcher et al. 1988; Kushnir and Lau 1992; Kushnir and Held 1996). In comparison, except for Palmer and Sun (1985), all high-resolution AGCMs have more than 18 levels. It remains unclear, however, if the vertical resolution is important for the difference between our R15 AGCM and other R15 AGCMs in, say, the simulation of eddy forcing. Clearly, much further study is needed to understand the key elements for the generation of the warm-ridge response.

4. The role of ocean–atmosphere coupling

We now investigate the atmospheric response in the presence of ocean–atmosphere coupling. To estimate the atmospheric response to a December SST anomaly dynamically in the coupled model, we performed a 40-member fully coupled ensemble (FCE) experiment. Each ensemble member starts from a 1 November atmosphere–ocean state of the CTRL plus a warm mixed layer temperature anomaly, with the 1 November state selected every 8 years apart in the CTRL. The temperature anomaly has the same bell shape as that in AMIP (Fig. 4) but extends uniformly to 200-m depth. (This mixed layer temperature anomaly can be thought as generated by anomalous ocean dynamics rather than by the atmospheric forcing.) Each ensemble member is then integrated for 2 months and the climate anomaly is obtained as the difference between each ensemble member run and the corresponding period of the CTRL. The initial value approach in FCE is effectively similar to the breeding method (Toth and Kalnay 1997) but in the coupled model. Now the ensemble atmospheric response emerges as the least damped coupled ocean–atmosphere mode (from November to December). As such, the atmospheric response to SST is considered from the coupled ocean–atmosphere perspective rather than the atmosphere-alone perspective.

The ensemble mean December atmospheric response in FCE shows a pronounced warm-ridge response (Figs. 7c,d), with a strong midlatitude surface easterly (Fig. 7a), an increased precipitation over the SST anomaly, and a decreased precipitation downstream (Fig. 7b). The pattern of the FCE atmospheric response resembles that of AMIP (Fig. 5) but with the magnitude almost doubled. This implies that ocean–atmosphere coupling increases the magnitude of the atmospheric response significantly but has little impact on the pattern of the response. This feature of a similar pattern but different amplitude can also be seen in the vertical structure of the geopotential height and temperature along the midlatitudes (Figs. 6a1,a2 versus Figs. 6b1,b2).

It is interesting that both the pattern and amplitude of the atmospheric response in FCE (Fig. 7) are consistent with the statistical estimation from the CTRL (Fig. 3). Since the AMIP response is about half the magnitude of the statistical estimation, FCE is clearly much more consistent with the statistical estimation than AMIP. This suggests that the FCE approach provides a better estimate of the atmospheric response than the traditional AMIP approach.

It is tempting to interpret the different atmospheric responses between FCE and AMIP in terms of the theory of Barsugli and Battisti (1998). In this theory, the SST variability in the coupled model is assumed to be generated by atmospheric internal variability, with a *downward* turbulent heat flux, driving the ocean but damping the atmosphere. Since SST is fixed in AMIP but follows the air temperature in the coupled experiment, coupling reduces the *downward* heat flux in the latter. This re-

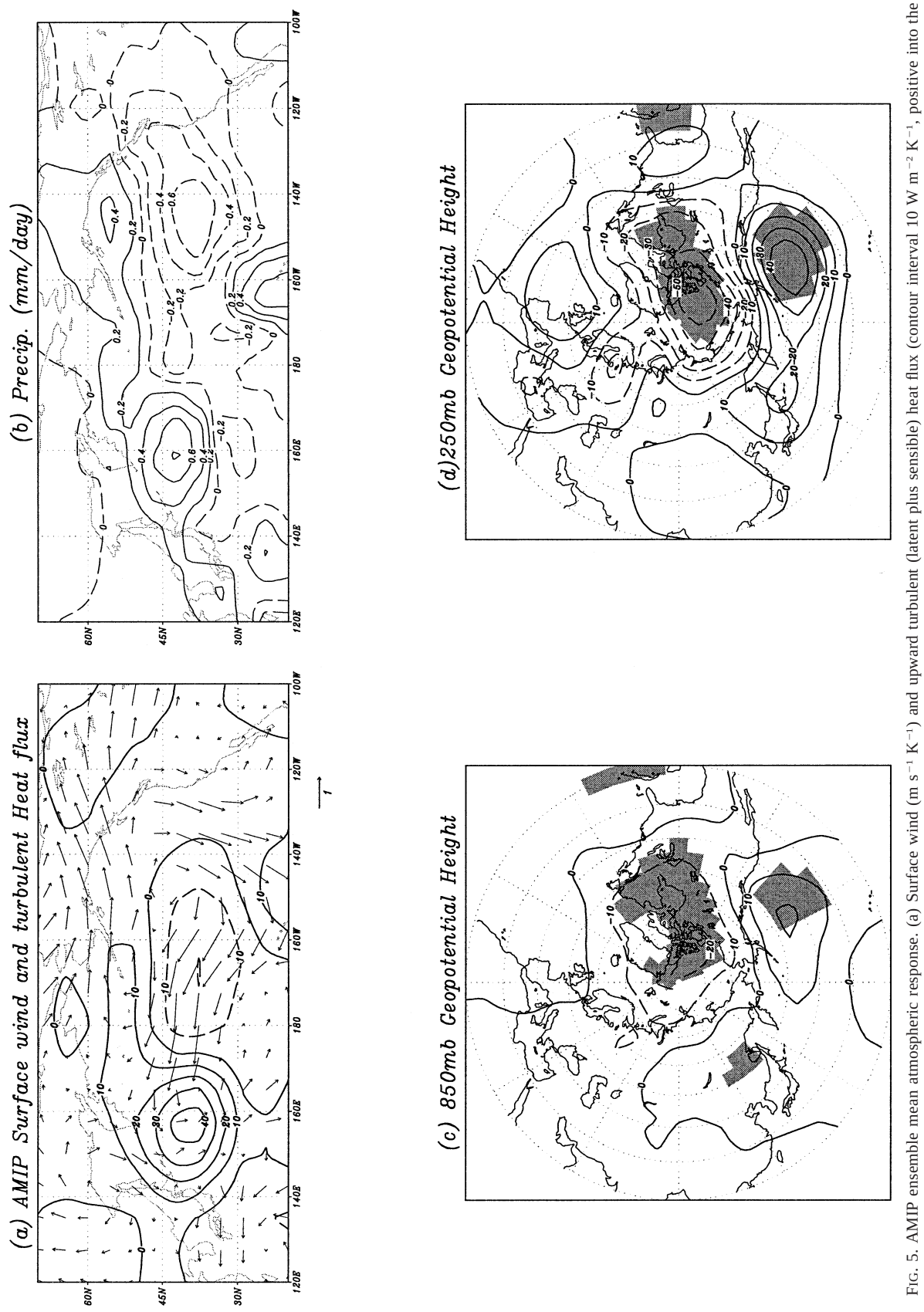

FIG. 5. AMIP ensemble mean atmospheric response. (a) Surface wind (m s^{-1} K^{-1}) and upward turbulent (latent plus sensible) heat flux (contour interval 10 W m^{-2} K^{-1}, positive into the atmosphere), (b) precipitation (contour interval 0.2 mm day^{-1} K^{-1}), (c) 850-hPa, and (d) 250-hPa geopotential height (contour interval 10 m K^{-1}). Negative contours are dashed. Shading indicates the ensemble mean statistically different from zero at the 95% level.

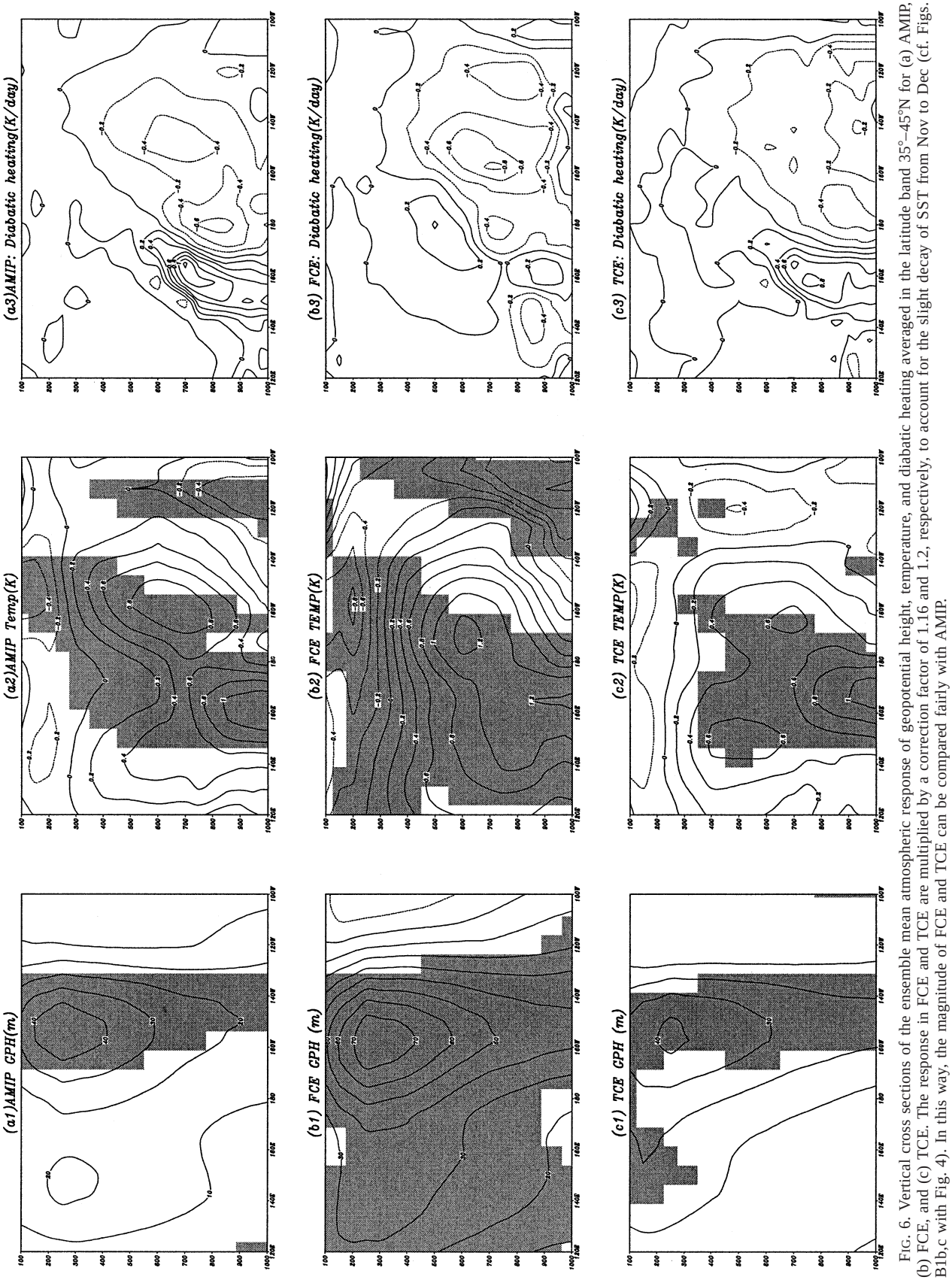

FIG. 6. Vertical cross sections of the ensemble mean atmospheric response of geopotential height, temperature, and diabatic heating averaged in the latitude band 35°–45°N for (a) AMIP, (b) FCE, and (c) TCE. The response in FCE and TCE are multiplied by a correction factor of 1.16 and 1.2, respectively, to account for the slight decay of SST from Nov to Dec (cf. Figs. B1b,c with Fig. 4). In this way, the magnitude of FCE and TCE can be compared fairly with AMIP.

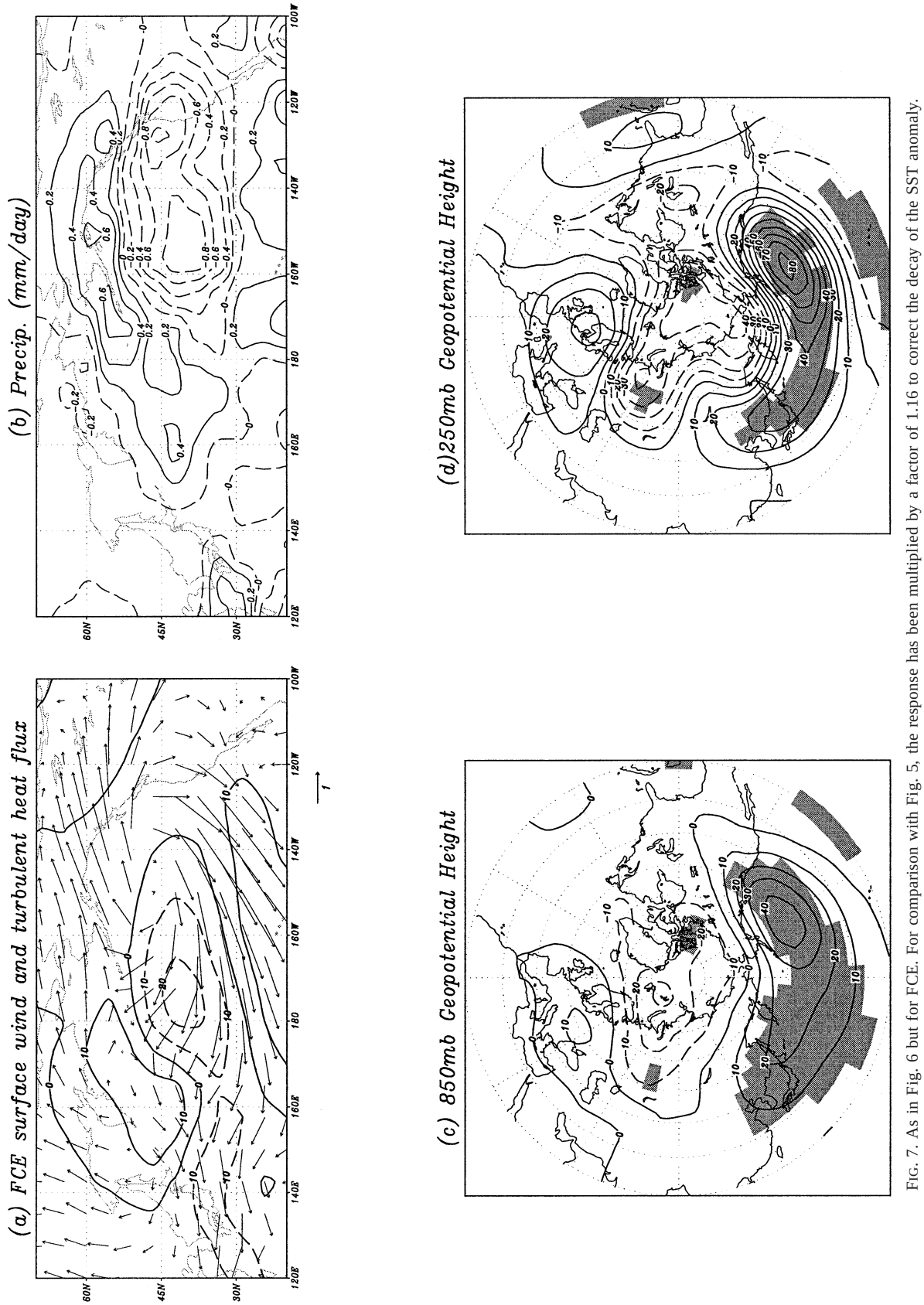

FIG. 7. As in Fig. 6 but for FCE. For comparison with Fig. 5, the response has been multiplied by a factor of 1.16 to correct the decay of the SST anomaly.

duction of downward heat flux reduces the damping to, and therefore enhances the variance of, the atmosphere in the coupled model relative to the AMIP.

The Barsugli and Battisti theory, however, does not apply to the FCE response here. This is because the SST anomaly in FCE is given a priori, presumably generated by ocean dynamics, instead of being forced by atmospheric internal variability. As a result, opposite to the scenario in Barsugli and Battisti, the heat flux is upward toward the atmosphere in the center of the SST anomaly (150°–170°E, positive in Figs. 5a and 7a), reflecting a forcing on the atmosphere but a damping of the SST. It is therefore interesting that, in spite of a stronger heat flux forcing on the atmosphere in AMIP than in FCE, the atmospheric response is weaker in the former. [The stronger thermal forcing in the former can be seen extending into the lower atmosphere over the SST anomaly due to a stronger precipitation (Fig. 5b versus Fig. 7b) and diabatic heating (Figs. 6a3 versus 6b3)]. A critical question is, therefore, why a stronger heat flux forcing in AMIP is associated with a weaker warm-ridge response. We will return to this question next.

5. Dynamic coupling and thermodynamic coupling

To further understand the role of coupling in atmospheric response, we performed a 60-member thermodynamically coupled ensemble (TCE) experiment. The TCE is the same as FCE except that the ocean momentum equations are forced by a prescribed seasonal cycle of wind stress (derived from the CTRL) rather than by the varying atmosphere above. As such, dynamic ocean–atmosphere coupling through wind stress forcing on the ocean is eliminated, while the thermodynamic coupling through the turbulent heat flux remains fully active as in FCE. The TCE is obtained similarly to FCE, with each member starting from a 1 November condition with a bell-shaped mixed layer temperature anomaly (Fig. 4). These 1 November states are taken from a 400-yr control run without dynamic coupling (CTRL-TCE).

Interestingly, the atmospheric response in TCE (Fig. 8) resembles closely that in AMIP (Fig. 5), both being characterized by a weak ridge downstream of the SST anomaly (Figs. 5c,d; Figs. 8c,d) and a strong positive heat flux and precipitation locally over the SST anomaly (Figs. 5a,b; Figs. 8a,b). In comparison, the response in FCE is twice stronger (Figs. 7c,d) but with half the local heat flux and precipitation (Figs. 7a,b). This feature of a similar pattern and different amplitude can again be seen in the vertical structures of the response along the midlatitudes (Fig. 6) as well as the thermodynamic and vorticity budgets (Figs. A1, A2). It should be pointed out that the similarity of the atmospheric responses in TCE and AMIP does not contradict the thermodynamic coupling theories of Barsugli and Battisti (1998) and Bretherton and Battisti (2000). As pointed out earlier, the SST anomaly is given here, rather than being forced by atmospheric internal variability as in these theories.

The three sets of ensemble experiments above suggest that it is the dynamic coupling, rather than the thermodynamic coupling, that enhances the atmospheric response to the midlatitude SST anomaly. It appears that the elimination of dynamic coupling results in a stronger local heat flux into the atmosphere. With a similar SST this stronger heat flux forcing is then, somehow, associated with a weaker warm-ridge response.

6. The role of coupling on atmospheric response

To understand the mechanism for the different atmospheric responses in TCE and FCE, we need to answer two questions. First, why does the elimination of dynamic coupling increase the heat flux into the atmosphere? Second, why is a stronger surface heat flux forcing, as in TCE and AMIP, accompanied by a weaker warm-ridge response? The surface heat budget may shed some light on the first question. Figure 9 shows the major terms for the SST equation in FCE and TCE. (For the oceanic heat budget here a positive surface heat flux is downward, warming the ocean.) Here, we only discuss the heat balance locally over the SST anomaly (east of 180°) (see appendix B for more discussion on the heat budget). The climatological heat balance for December SST is dominated by a surface heat loss (negative) and convective warming (positive) (not shown). In FCE (Fig. 9a), the addition of the warm SST anomaly results in an excessive heat loss to the atmosphere (negative), which is balanced mainly by an anomalous meridional advection $v'\overline{T}_y$ (positive averaged over the SST anomaly); this warm advection is mainly associated with the anomalous northward Ekman flow, which is forced by the anomalous surface easterly that is a part of the atmospheric response to the anomalous SST. Therefore, the anomalous Ekman flow together with the warm-ridge response forms a positive feedback on the SST anomaly and contributes significantly to the SST heat budget. (Overall, however, this positive Ekman flow feedback is overwhelmed by the negative feedback due to the surface heat flux.) This positive feedback, however, is eliminated in TCE (Fig. 9b) because of the suppression of dynamic coupling. Now, the absence of an advective warming of Ekman flow induces a stronger surface cooling, which destabilizes the surface ocean and leads to a stronger convective warming. This convective warming is balanced by a much stronger surface heat loss. Therefore, the elimination of dynamic coupling in TCE suppresses a positive feedback on SST or, equivalently, enhances the damping of the SST anomaly and therefore should contribute to the enhanced upward heat flux into the atmosphere. As another evidence of the role of changed feedback affecting the atmospheric response, we notice that the November response in FCE and TCE are very similar; both have a strong upward surface heat flux with no significant atmospheric responses (not shown). This implies that the December atmospheric responses in both FCE and TCE fully de-

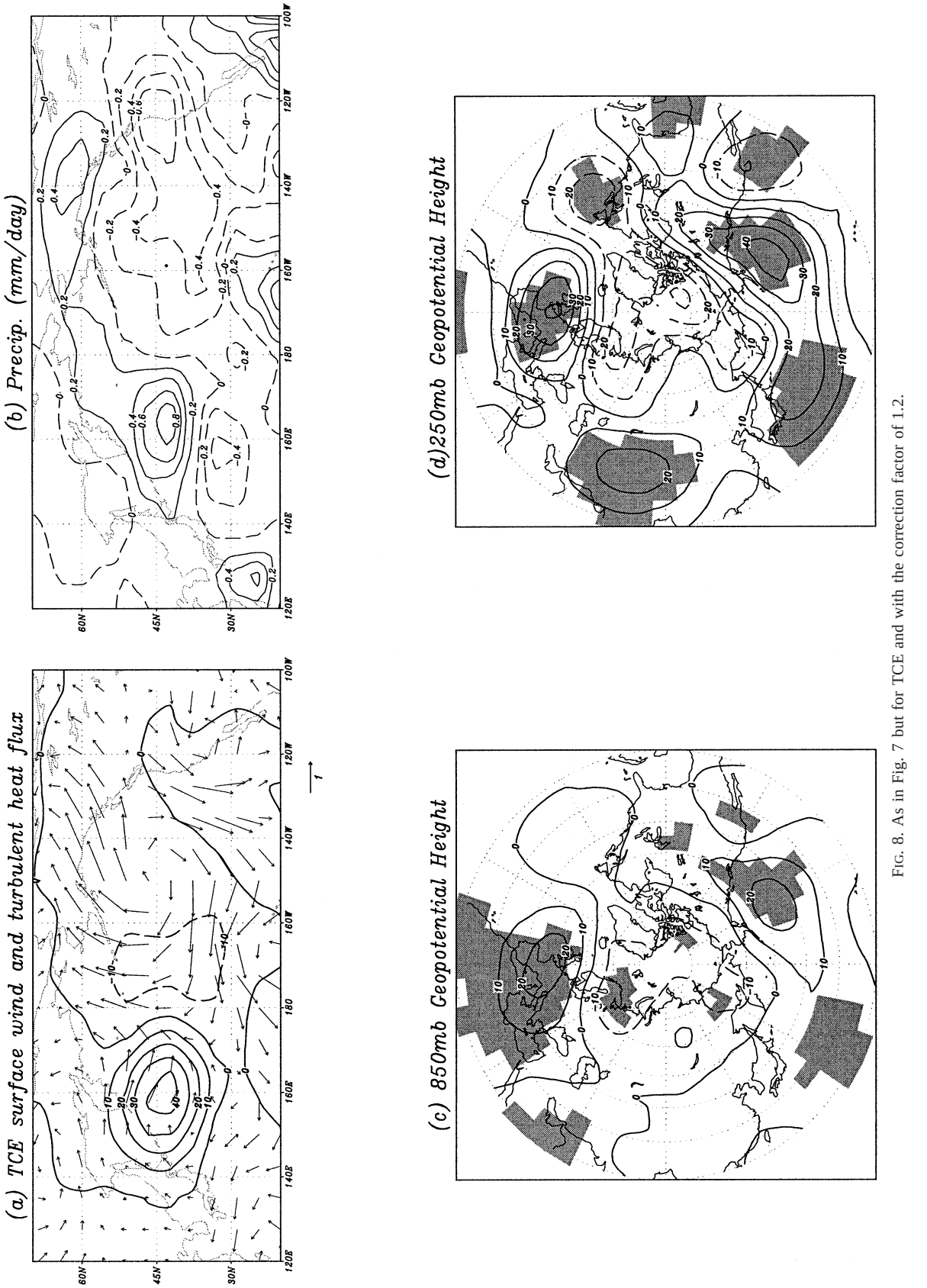

FIG. 8. As in Fig. 7 but for TCE and with the correction factor of 1.2.

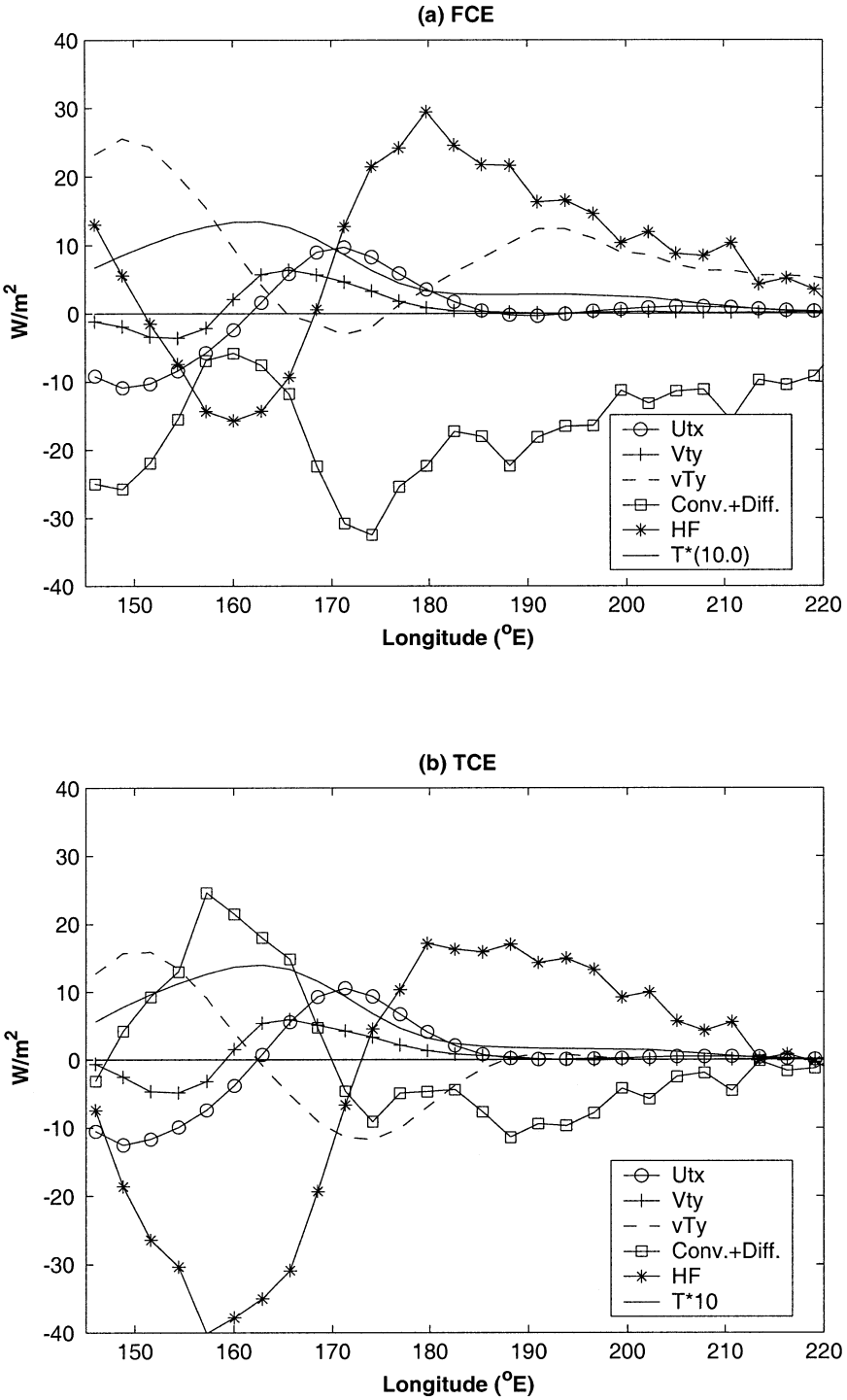

FIG. 9. Ensemble mean Dec SST (upper 50-m average) tendencies induced by each term of the SST equation in the latitude band 35°–45°N: (a) FCE and (b) TCE. Mean zonal advection (circle), mean meridional advection (plus), perturbation meridional advection (dash), convection and vertical diffusion (square), surface heat flux (star), and temperature multiplied by 10 (solid). Not plotted are small terms of perturbation zonal advection and mean and perturbation vertical advection.

velop only after a finite time (about a month), which is longer than the short (presumably a week long) atmospheric response time. This development time is long enough to allow the coupled process to impact the atmospheric response, including the transient eddies.

Now, we turn to the second question, which is a much more fundamental yet difficult question: why is a stronger heat flux forcing associated with a weaker warm-ridge response? For convenience, let us first think of the strong upward heat flux anomaly in TCE (or AMIP) as the sum of the weak upward heat flux anomaly of FCE and an additional upward heat flux anomaly forcing to the atmosphere. If our atmosphere responds to the additional heat flux with a downstream low (warm-low response), as in Yulaeva et al. (2001) and Sutton and Mathieu (2002), the atmospheric response in TCE may be thought as the sum of the strong warm-ridge response of FCE and the warm-low response forced by the additional heat flux; the latter response cancels part of the former response and, therefore, results in a weak warm-ridge response in TCE. This reasoning leads us to hypothesize that the atmospheric response in TCE can be thought as the sum of the FCE response and a upward flux-forced response. Equivalently, the atmospheric response in FCE can be thought as the sum of the TCE response and a downward-flux-forced response.

As a support for our hypothesis, further FOAM experiments show that an upward heat flux can indeed force a warm-low response. We performed an additional 40-member flux forced ensemble (FXE) that is forced by an anomalous heat flux as in Yulaeva et al. (2001) and Sutton and Mathieu (2002), but in the fully coupled FOAM. Each ensemble member starts from a 1 November condition of the CTRL and is forced by a constant upward heat flux anomaly. The heat flux anomaly is bell shaped and is located in the Kuroshio Extension region, similar to the SST anomaly in Fig. 4. The maximum heat flux is 30 W m^{-2}, chosen to be comparable with the heat flux difference between TCE (or AMIP) and FCE. The atmospheric response in FXE is indeed dominated by a downstream low, an increased westerly, and precipitation in the midlatitudes (Fig. 10). This result is consistent with Yulaeva et al. (2001) and Sutton and Mathieu (2002). Even more amazing is that, quantitatively, the sum of the atmospheric responses in FCE (Fig. 7) and FXE (Fig. 10) almost equals the atmospheric response in TCE (Fig. 8). For example, the maximum 250-hPa height anomaly is 80 m in FCE (Fig. 7d) and −40 m in FXE (Fig. 10d), with a sum of 40 m. This sum almost equals the 40-m response in TCE (Fig. 8d).

The analysis above leads us to conclude that the December atmospheric response depends not only on the SST itself but also on the heat flux forcing. A warm SST forcing (accompanied by a weak flux) tends to generate a warm-ridge response, while a warm heat flux (accompanied by a small SST anomaly) tends to generate a warm-low response. A fully coupled model (FCE) produces the correct response as obtained from the statistical estimation because its full coupling process generates the correct combination of SST and heat flux forcing, naturally. Both the AMIP and TCE, however, tend to generate too large a heat flux forcing, leading to a weak warm-ridge response.

The discussion above regards the SST and heat flux forcing as if they are independent. This view seems to give a consistent interpretation of our model atmospheric response and is therefore helpful for our understanding of the role of coupling in atmospheric response. However, physically SST forces the atmosphere through the surface heat flux and therefore is not independent of the heat flux. The view above, therefore, still leaves it open as to why the SST forcing and heat flux forcing acts on the model atmosphere as if they are independent. This question is still unclear to us.

It is possible that the seemingly independent roles of SST and heat flux forcing, as discussed above, is a result, rather than the cause, of the atmospheric response. The atmospheric response, instead, is caused by some other mechanism. Of particular importance, as suggested by one reviewer, is the feedback of atmospheric eddy forcing. Recent GCM studies suggested that an extratropical SST anomaly induces two main forcings: a direct forcing associated with diabatic heating and an indirect forcing associated with the eddy vorticity forcing (Peng et al. 1997; Peng and Whitaker 1999; Peng and Robinson 2001). The eddy vorticity forcing results initially from the interactions between the heating-forced flow and the storm tracks but then, in turn, substantially modify the heating and become dominant in sustaining the warm-ridge response. As seen in the temperature anomalies (Figs. 6a2,b2,c2) and the corresponding thermodynamic budget (Fig. A1), the shallow warm temperature center locally over the SST anomaly is forced directly by a corresponding diabatic heating center there. In contrast, the midair warming center in the downstream is damped by a diabatic cooling center and therefore is not a direct response to the diabatic heating. Instead, it results from the adjustment to the eddy vorticity forcing. One possibility is that the SST anomaly induces a northward shift in the Pacific storm track; the resulting negative eddy vorticity forcing would drive the warm-ridge response. [This negative vorticity forcing can be seen in the vorticity budget in the residual vorticity forcing on 850 hPa (Figs. A2a3,b3,c3). This negative residual vorticity forcing becomes even more clear for the column averaged vorticity budget, where the only negative vorticity forcing in the downstream is the residual forcing (not shown).] Both the low-level warming and anomalous easterlies associated with the ridge tend to minimize the upward heat flux over the SST anomaly. A strongly eddy-induced ridge response, as in FCE, would therefore result in a weak heat flux, while a weakly eddy-induced ridge response, as in AMIP and TCE, would correspond to a strong heat flux. In this view, the different heat flux in the different experiments are

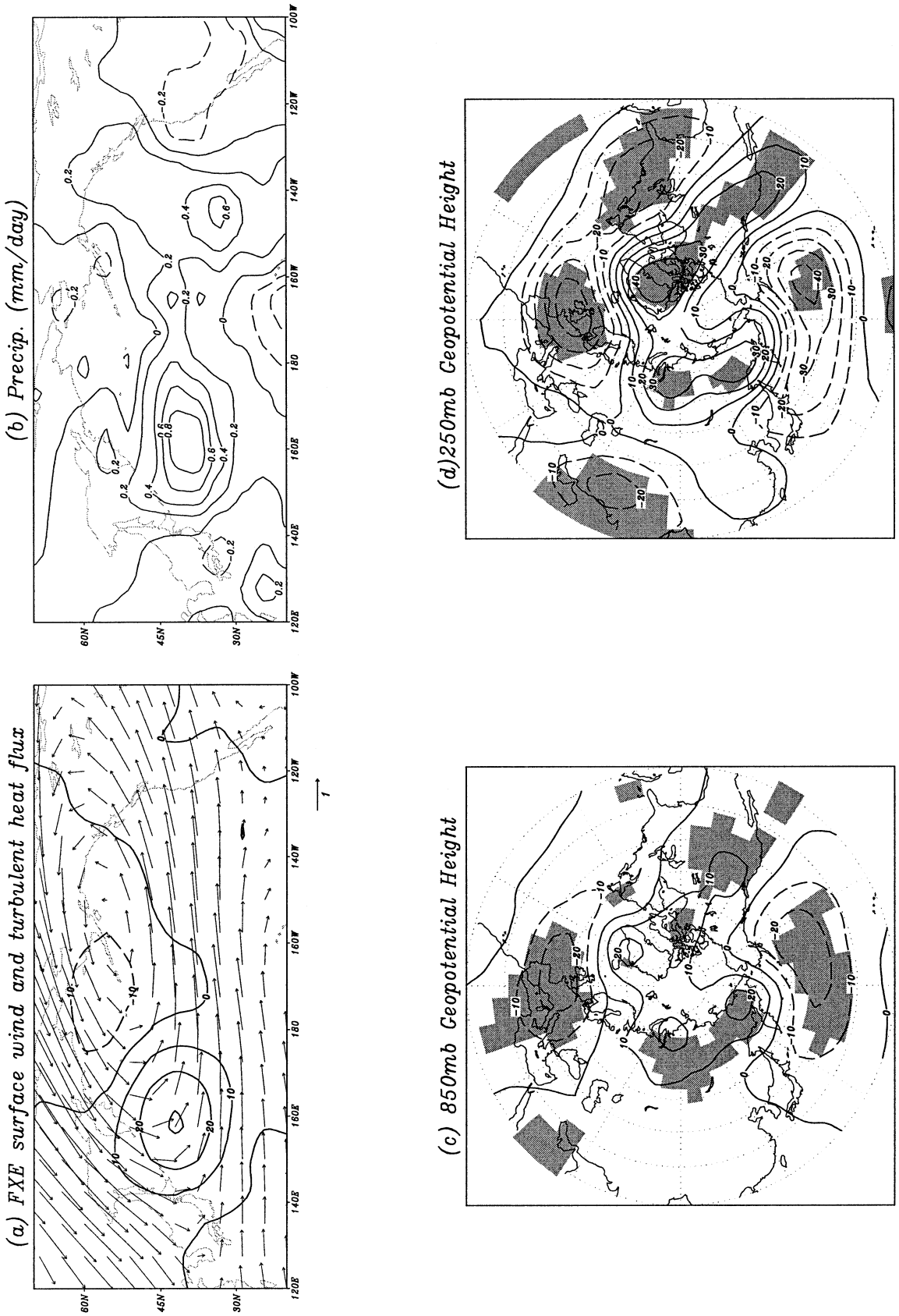

FIG. 10. As in Fig. 7 but for FXE.

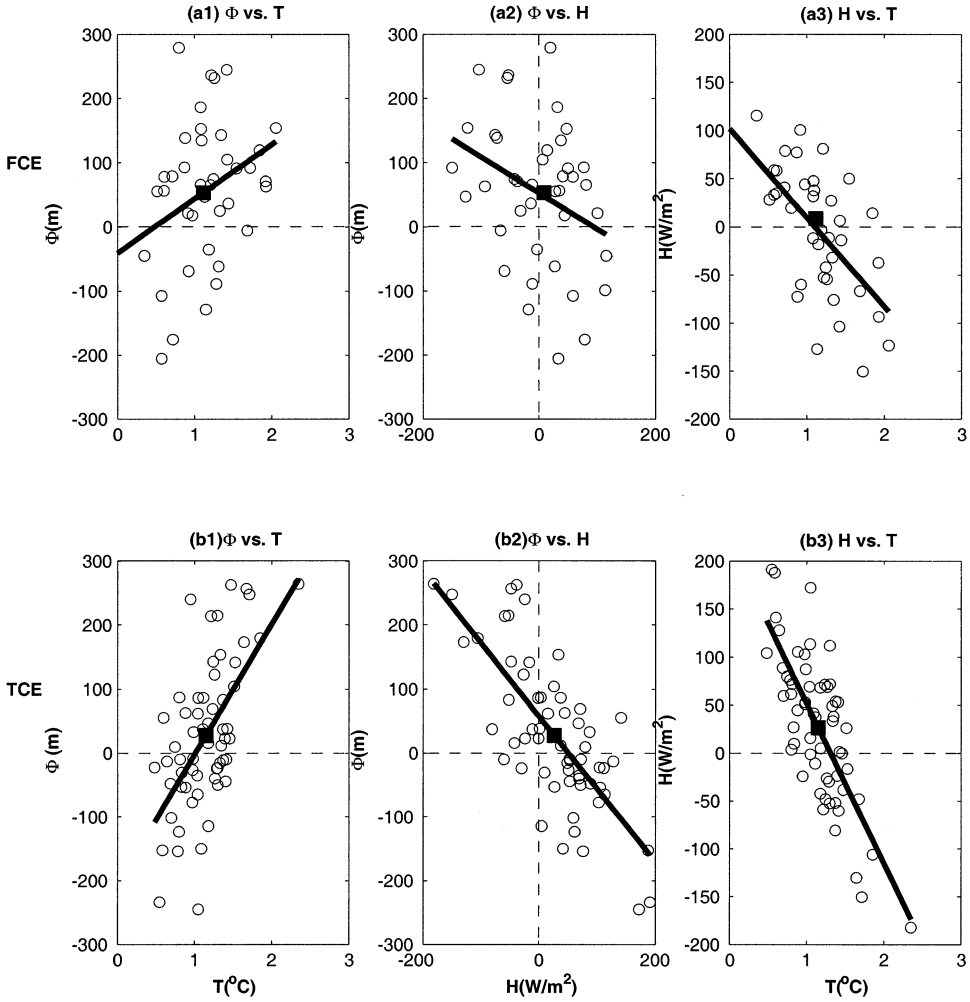

FIG. 11. Ensemble scattering diagram of the Dec anomalous atmosphere 500-hPa geopotential height, SST, and upward turbulent heat flux in (a) FCE and (b) TCE. Each variable is averaged the same as in Table 1. The three variables are plotted in three pairs: height–SST, height–heat flux, and heat flux–SST. Each circle represents one ensemble member, and the solid square is the ensemble average response. The heavy line is the regression line for the scattering. The regression coefficient, correlation coefficient, and ratio of ensemble means for each pair of variables are also calculated in Table 1.

the results rather than the cause. If this eddy view is more correct, the key question is, therefore, why the full coupling in FCE leads to a much stronger perturbation of the Pacific storm track. To answer this question further study of the role of coupling on the intrinsic variability of the atmosphere would be required, which cannot be addressed here because all of our model outputs are saved in monthly averages with no direct information on high-frequency atmospheric variability. We therefore defer the role of eddy forcing for future studies.

7. Atmospheric forcing, response, and atmosphere–ocean feedback

Our discussion so far is limited to the atmospheric response to the ocean. To further shed light on ocean–atmosphere feedback we now examine both the atmospheric forcing on the ocean and the atmospheric response to the ocean together.

In the ensemble experiments, the effect of atmospheric forcing can be distinguished from that of the atmospheric response by considering the ensemble scattering and ensemble mean separately. This follows because the scattering among the ensemble members reflects the ''noise'' of atmospheric forcing on the ocean, while the ensemble mean represents the ''signal'' of the atmospheric response to the ocean. Figure 11 shows the scattering diagram of anomalous SST, 500-hPa geopotential height, and upward heat flux in FCE (Fig. 11a) and TCE (Fig. 11b), all averaged in the Kuroshio Extension region. One general feature in Fig. 11 is the large scatter among the ensemble members (circles) relative to the ensemble mean (solid square). This implies

TABLE 1. Atmosphere–SST sensitivity $\partial\Phi/\partial T$ (m K^{-1}), atmosphere–heat flux sensitivity $\partial\Phi/\partial H$ m (W m^{-2}), and heat flux–SST sensitivity $\partial H/\partial T$ (W m^{-2} K^{-1}), estimated from the anomalous 500-hPa geopotential height Φ, SST T, and upward turbulent heat flux H. The variables are averaged in the Kuroshio Extension region (35°–45°N, 140°E–180°) for T and H, but in the downstream region (35°–50°N, 180°–140°W) for Φ. For each set of ensemble experiments, the forcing sensitivity is estimated as the regression coefficient (Reg) of the ensemble member scattering, with the response sensitivity as the ratio of the ensemble means. For each forcing sensitivity, the correlation coefficient (Corr; in parentheses) indicates the level of scattering. Correlations and ensemble means that are statistically different from zero at the 95% significance level are in bold.

Sensitivity	Forcing $\partial\Phi/\partial T$ Reg (Corr)	Response $\partial\Phi/\partial T$ $E(\Phi)/E(T)$	Forcing $\partial\Phi/\partial H$ Reg (Corr)	Response $\partial\Phi/\partial H$ $E(\Phi)/E(H)$	Forcing $\partial H/\partial T$ Reg (Corr)	Response $\partial H/\partial T$ $E(H)/E(T)$
FCE	84 (0.36)	**53/1.2**	−0.56 (−0.33)	**53/9**	−92 (**−0.65**)	**9/1.2**
TCE	203 (**−0.6**)	**27/1.2**	−1.13 (**−0.74**)	**27/26**	−167 (**−0.75**)	**26/1.2**
AMIP			−0.72 (**−0.63**)	**28/20**		
FXE	83 (**0.50**)	**−22**/0.1	−0.55 (−0.33)	**−22/26**		

a dominant atmospheric forcing on the ocean. In other words, the atmospheric response to the ocean is a small signal relative to the noise of internal atmospheric variability.

For the FCE, the scattering diagrams are plotted in three pairs: height–SST (Fig. 11a1), height–heat flux (Fig. 11a2), and heat flux–SST (Fig. 11a3), which will be used to calculate the atmosphere–SST sensitivity $\partial\Phi/\partial T$, atmosphere–heat flux sensitivity $\partial\Phi/\partial H$, and heat flux–SST sensitivity $\partial H/\partial T$, respectively. Each sensitivity has a pair of values: one for the atmospheric forcing on the ocean and the other for the atmospheric response to the ocean, hereafter referred to as forcing sensitivity and response sensitivity, respectively. The forcing sensitivity is calculated as the regression coefficient of the ensemble scattering, with the response sensitivity as the ratio of the two ensemble means (Table 1). The forcing sensitivity and the response sensitivity are generally different (Table 1) because they represent different physical processes.

The atmospheric forcing, or the scattering, in FCE is characterized by a positive $\partial\Phi/\partial T$, a negative $\partial\Phi/\partial H$, and a negative $\partial H/\partial T$ (Table 1) representing a warmer SST/higher pressure (Fig. 11a1), a weaker upward flux/higher pressure (Fig. 11a2), and a warmer SST/weaker upward flux (Fig. 11a3), respectively. This correlation of warmer SST/higher pressure/weaker upward flux can be understood in terms of the forcing of the atmospheric internal variability on the ocean. An internal atmospheric variability of, say, an equivalent barotropic high (higher pressure) weakens the Aleutian low and in turn the surface westerly wind in the midlatitudes; the weaker westerly increases the SST (warmer SST) by reducing the turbulent heat flux into the atmosphere (weaker upward flux) and inducing a northward warm Ekman advection (not shown).

The atmospheric response to the ocean, or the ensemble mean, in FCE is also characterized by a positive $\partial\Phi/\partial T$ (Table 1, Fig. 11a1) corresponding to a warm-ridge response as discussed before. The fact that the forcing $\partial\Phi/\partial T$ is of the same sign as the response $\partial\Phi/\partial T$ implies a positive feedback between the atmospheric height and SST: a warm SST forces a high pressure (response $\partial\Phi/\partial T > 0$), which weakens the westerly surface wind in the midlatitudes and therefore further warms the SST (forcing $\partial\Phi/\partial T > 0$).

The heat flux–SST sensitivity $\partial H/\partial T$ is positive for the response (Table 1, Fig. 11a3). This positive response $\partial H/\partial T$ is of the opposite sign to the negative forcing $\partial H/\partial T$, implying a negative feedback between the SST and heat flux (Frankignoul et al. 2002). Physically, a positive heat flux is induced by a warmer SST that is given a priori in FCE (response $\partial H/\partial T > 0$); the increased heat flux into the atmosphere means an enhanced heat loss of the surface ocean and then a reduction of the initial SST forcing ($\partial H/\partial T < 0$).

The atmosphere–heat flux sensitivity $\partial\Phi/\partial H$ is positive for the atmospheric response (Table 1, Fig. 11a2) because the warm-ridge response (Figs. 6c,d) is accompanied by an increased heat flux into the atmosphere (Fig. 6a). In contrast to $\partial\Phi/\partial T$, this positive response $\partial\Phi/\partial H$ is of the opposite sign to the forcing $\partial\Phi/\partial H$ and therefore implies a negative feedback between the atmosphere and surface heat flux. Physically, an upward heat flux response is induced by a warmer SST in FCE and the warmer SST generates a higher pressure as a warm-ridge response. This leads to a positive response $\partial\Phi/\partial H(> 0)$. The higher pressure, however, tends to reduce the westerly wind, and in turn the heat flux into the atmosphere (forcing $\partial\Phi/\partial H < 0$), reducing the initial upward heat flux.

The sensitivities in TCE are qualitatively similar to those in the FCE (Table 1, Fig. 11b), representing a qualitatively similar atmospheric response, atmospheric forcing, and ocean–atmosphere feedback. The similarity of the atmospheric responses has been discussed in sections 4 and 5. Quantitatively, however, the response $\partial\Phi/\partial T$ is twice stronger in FCE than in TCE, while the response $\partial H/\partial T$ is twice stronger in TCE than in FCE. These represent the stronger heat flux and weaker warm-ridge response in TCE than in FCE, as discussed before. Furthermore, both the forcing $\partial\Phi/\partial T$ and forcing $\partial H/\partial T$ are about twice stronger in TCE than in FCE. This occurs because in TCE the elimination of the positive feedback associated with Ekman advection results in an enhanced negative ocean–atmosphere feedback. As a result, to force the same magnitude of SST change the atmospheric forcing or heat flux forcing needs to be

twice stronger in TCE than in FCE. The stronger negative ocean–atmosphere feedback in TCE also results in a much smaller scatter of the atmospheric noise than in FCE, as seen by comparing Fig. 11b with Fig. 11a. Indeed, the correlation coefficients for the three forcing sensitivities in TCE are all above 0.6 and statistically significantly from zero at the 95% level (Table 1). These are substantially higher than those in FCE, which can reach below 0.4 and are not statistically different from zero (Table 1).

Finally, we can also calculate some sensitivity for AMIP and FXE (Table 1, scattering diagrams not shown). Most interesting is the FXE. Now, both the forcing $\partial\Phi/\partial T$ and forcing $\partial\Phi/\partial H$ are virtually identical to those in FCE (Table 1) because they represent the same forcing process of atmospheric internal variability on the ocean with the same ocean–atmosphere feedback conditions in the two ensembles. However, the sign of both the response $\partial\Phi/\partial T$ and response $\partial\Phi/\partial H$ become negative, opposite from all the other cases (Table 1). This occurs because of the warm-low response in response to the heat flux forcing. As a result, opposite to FCE, the forcing $\partial\Phi/\partial T$ and response $\partial\Phi/\partial T$ are of opposite sign while the forcing $\partial\Phi/\partial H$ and response $\partial\Phi/\partial H$ are of the same sign, implying a negative atmosphere–SST feedback and positive atmosphere–flux feedback. Therefore, the feedback between the atmosphere and ocean depends on the way that the atmosphere is forced. In FCE (or TCE), the forcing is the SST (see later Figs. B1b,c) while the heat flux is a by-product; the feedback is positive between the atmosphere and SST but negative between the atmosphere and heat flux. In contrast, in FXE, the forcing is the heat flux while the SST is a small by-product (see later Fig. B1d). The feedback is positive between the atmosphere and heat flux but negative between the atmosphere and SST.

8. Summary and discussions

A first attempt is made to study the atmospheric response to a midlatitude winter SST anomaly in a coupled ocean–atmosphere general circulation model. Unlike previous studies that tend to focus on atmospheric dynamics, especially the atmospheric eddy forcing (e.g., Peng et al. 1995, 1997; Peng and Whitaker 1999; Peng and Robinson 2001), we have focused on the role of ocean–atmosphere coupling. A new approach is used here to understand the role of coupling in the atmospheric response using ensemble coupled experiments of different coupling configurations. The ensemble atmospheric responses are also compared with a statistic estimation of the control simulation (CTRL). The main conclusion is that the atmospheric response depends not only on the SST anomaly but also on the surface heat flux forcing. The SST and heat flux seem to generate opposite responses, with the SST favoring a warm-ridge response and the heat flux favoring a warm-low response. The correct atmospheric response is generated in the fully coupled ensemble (FCE) in which a correct combination of SST and heat flux is generated naturally.

Specifically, FCE produces the strongest warm-ridge response but is accompanied by a weak upward heat flux. This response agrees best with the statistical estimation from the CTRL simulation. The AMIP ensemble generates a warm-ridge response, as in most previous high resolution models; so does the thermodynamically coupled ensemble (TCE). However, the magnitudes of the response in these latter two ensembles are only half that of the FCE. The weaker warm-ridge response in AMIP and TCE are found to be associated with excessive heat flux forcing to the atmosphere. (In TCE, this excessive heat flux is found to be related to the elimination of the positive dynamic ocean–atmosphere feedback associated with Ekman advection.) This anomalous heat flux forcing generates a warm-low response, as shown in FXE. The warm-low response cancels part of the warm-ridge response of FCE and eventually leads to a weaker warm-ridge response in AMIP and TCE.

Further studies are carried out on the feedback between the atmosphere and ocean. For the SST-forced ensembles (FCE, TCE, and AMIP), the atmospheric response forms a part of the positive atmosphere–SST feedback, which is then damped by a negative atmosphere–heat flux feedback. To the contrary, for the flux-forced ensemble (FXE), the atmospheric response forms a positive atmosphere–heat flux feedback, but is damped by a negative atmosphere–SST feedback.

In the following, we discuss some further issues.

a. Forcing to the atmosphere

Our attention on ocean–atmosphere coupling is partly motivated by the recent debate whether the atmospheric response to a midlatitude oceanic climate anomaly should be studied using a fixed SST forcing (AMIP) or a fixed heat flux forcing (FXE). Our study suggests that the atmospheric response depends on both SST and heat flux forcing. Therefore, neither AMIP nor FXE is correct. Instead, the correct response of the atmosphere seems to be generated in FCE in which the SST and flux are adjusted naturally through the full coupling process. The distortion of the coupling process, such as in TCE, reduces the atmospheric response substantially.

Within the context of AMIP and FXE only, AMIP appears to be more correct than FXE. This follows because FXE generates a warm-low response that is the opposite to the true response in FCE (or statistical estimation). In comparison, the AMIP response is more consistent with the true response, both being a warm-ridge response. This conclusion, however, may only apply to atmospheric responses of monthly time scales because both the responses from the statistical analysis and the FCE are for monthly time scales. At monthly time scale, it is also easy to understand why the AMIP

resembles the FCE more than the FXE. The fixed SST in AMIP assumes an infinite heat capacity of the ocean (Saravanan and Chang 1999; Yulaeva et al. 2001; Sutton and Mathieu 2002). This assumption of a large heat capacity is a reasonable approximation at monthly time scales, especially in winter when the mixed layer is deep. Therefore, AMIP resembles the FCE much better than the FXE. This further explains why AMIP resembles TCE even more than FCE does. In TCE, the lack of the positive feedback associated with the dynamic coupling enhances the overall negative ocean–atmosphere feedback and generates less SST variability. Thus, the TCE becomes more similar to the AMIP case; in the latter case fixed SST is known to generate excessive damping to the atmosphere.

It is important to point out that the view above tends to regard the SST forcing and heat flux forcing independently. This view, while perhaps convenient for shedding light on the different atmospheric responses, is somewhat problematic. As discussed at the end of section 6, the SST forces the atmosphere through the heat flux and therefore is not completely independent from the heat flux forcing. It remains to be understood why in our case here the atmospheric response can be interpreted as if the SST forcing and heat flux forcing are independent.

Finally, our initial value approach in FCE and TCE is equivalent to the ''breeding'' method (Toth and Kanley 1997) that favors the slowest decaying coupled ocean–atmosphere mode. This suggests that the atmospheric response may be viewed alternatively from a coupled ocean–atmosphere modal evolution perspective. This coupled perspective may provide a different view that is perhaps more effective than the classical view of the ''forced atmospheric response.''

b. Statistical estimation

It remains challenging to assess the atmospheric response accurately from the observation, or a coupled control simulation. An instantaneous covariance between the atmosphere and SST is improper for the extraction of the atmospheric response signal because of the dominant variability forced by the atmospheric internal variability (Frankignoul et al. 1998). We have made use of the SST-lead regression to filter out the atmospheric-forced variability, a method originally proposed for the study of local air–sea heat flux feedback by Frankignoul et al. (1998). This method is subject to statistical and dynamic constrains as well as sampling noises and, therefore, should be regarded with caution. Furthermore, the atmospheric response is nonlocal. The application of this method to identify the atmospheric response has the additional difficulty of distinguishing nonlocal atmospheric responses. A combination of multivariate analysis and SST-lead covariance may be a step forward (Cajza and Frankignoul 2002), but its effectiveness remains unclear. The dynamic assessment, like our modeling study here, is therefore important because it is complementary to any statistical assessment. In our case here for the atmospheric response to a midlatitude North Pacific SST anomaly, the statistical estimation gives a similar response to the dynamic response in FCE. If this similarity is true for other problems, however, remains to be seen.

c. Remote response over North Atlantic/Europe sector

Our study also shows a significant remote ridge response over the North Atlantic/Europe sector in response to the warm SST anomaly in the western North Pacific. This remote ridge response can be seen clearly in the statistical estimation of the NCEP–NCAR reanalysis (Fig. 2) and the model CTRL (Fig. 3). This remote response is also produced clearly in our ensemble experiments, strongest in FCE (Figs. 7c,d) and modest in TCE (Figs. 8c,d) and AMIP (Figs. 5c,d). There is also a similar remote response in FXE, but with opposite sign, as for the local North Pacific response (Figs. 10c,d). The consistency between the statistical estimation and our dynamic model responses suggests that this remote response is a robust dynamic remote response of the North Atlantic/Europe sector to the SST anomaly in the western North Pacific. This remote response may be important for understanding the dynamics of the combined climate variability in the North Pacific and North Atlantic, as discussed in recent works (e.g., Thompson and Wallace 1998; Deser 2000).

This work is a first attempt to use a fully coupled model to study the atmospheric response to midlatitude SST. Many issues, therefore, require further studies. We have studied the atmospheric response to a December western North Pacific SST anomaly. The response of the atmosphere could differ for SST variability at different locations and for different months. Two additional sets of FCE-type ensemble experiments are performed. In the first ensemble, the mixed layer temperature anomaly is located in the central North Pacific. The warm-ridge response is much reduced. This suggests that the location of the SST anomaly is also important. Previous studies have described the atmospheric response to North Pacific SST anomaly in different regions. Part of the difference among these studies may be caused by different locations of the SST anomalies.

The second ensemble examines the atmospheric response in November, with each ensemble member starting from a 1 October ocean–atmosphere state. The November atmospheric response is again substantially weaker than the December response. This weaker November atmospheric response is consistent with the statistical estimation of the CTRL (Fig. 1b). This seasonal dependence of the atmospheric response may be caused, however, not only by the different seasonal atmospheric climatology (Peng et al. 1995) but also by different seasonal mixed layers. The weaker November response seems to be at least partly attributed to a shallower

mixed layer. The decay of SST from October to November is found to be stronger than that from November to December because of a shallower mixed layer and in turn shorter SST persistence in November. As a result, the atmospheric response is forced by a smaller SST anomaly in November than in December. This seasonal dependence of the atmospheric response to ocean mixed layer depth can occur in a coupled model, but not in an AGCM or a coupled AGCM–slab mixed layer model. The relative roles of these two seasonal effects in the real world, however, remains to be studied.

One deficiency of this paper is the lack of study of the role of the intrinsic atmospheric variability. It is conceivable that atmospheric eddies could contribute substantially to different responses in our experiments here. One should also notice that this eddy-forcing view, however, may not be inconsistent with our view of SST/flux forcing because ocean–atmosphere coupling may also affect the evolution of atmospheric eddies themselves and therefore lead to different ensemble mean responses (see the end of section 6). All of these effects of feedback with the atmospheric eddy forcing will need to be studied in the future.

Acknowledgments. We thank Dr. R. Jacob for his continued development of FOAM, Dr. R. Gallimore for his help on the development of the coupling scheme, Dr. E. DeWeaver for some discussions on atmospheric dynamics, and Ms. D. Lee and Dr. Q. Zhang for their analysis of the observation and CTRL simulation. We also thank the useful comments from two anonymous reviewers and Dr. W. Robinson on an earlier version of the paper. The computation is performed at SCD NCAR, and NCAR is supported by the National Science Foundation.

APPENDIX A

Thermodynamic and Vorticity Budgets

The thermodynamic and vorticity budget of our ensembles are similar to Peng et al. (1997) and are presented here for completeness. Following Peng et al. (1997), the thermodynamic and vorticity budgets are constructed using the monthly mean variables according to

$$u\frac{\partial\theta}{\partial x} + v\frac{\partial\theta}{\partial y} + \omega\frac{\partial\theta}{\partial p} = Q \quad \text{and} \tag{A1}$$

$$u\frac{\partial\zeta}{\partial x} + v\frac{\partial\zeta}{\partial y} + \beta v = (\zeta + f)\frac{\partial\omega}{\partial p} + R. \tag{A2}$$

The thermal forcing Q represents mainly the diabatic heating and the convergence of submonthly transient eddy heat flux, while the vorticity residual R should represent predominantly the convergence of submonthly transient eddy vorticity flux. The anomalous heat budget of AMIP is plotted for zonal advection, meridional advection, vertical advection, and the thermal forcing along 40°N in the vertical section (Fig. A1a). Similar to Fig. 13 of Peng et al. (1997), the zonal advection is dominated by a cold advection in the west and a warm advection in the east separated by an upper-air temperature maximum at 160°W (Fig. 6a2). The zonal advection is largely compensated by the meridional advection, which can be further shown to be dominated by the anomalous advection associated with the ridge response: northward warm advection in the west and a southward cold advection in the east (not shown). The lack of meridional temperature advection by the climatological mean wind has been speculated to contribute to the warm-ridge response (Peng et al. 1997). The vertical advection is important in the upper level, dominated by cold air ascending in the west and warm air descending in the east, while the residual forcing is a heating to the west and cooling to the east. These major features of the heat budget in AMIP are also present in FCE (Fig. A1b) and TCE (Fig. A1c), while the intensity seems to be the strongest in the FCE.

The vorticity budget of AMIP is shown for advection, divergence, and residual forcing at 850 hPa (Fig. A2a). The 850-hPa wind vectors are also shown in Fig. A2a. Similar to Fig. 9 of Peng et al. (1997), the budget is dominated by the vorticity divergence term. The stretching (negative) east of 150°W and compression (positive) in the west are associated with the ascending and descending upper-air motion, respectively. The vorticity divergence is balanced by the advection and residual terms. The advection term is dominated by the planetary advection, northward (positive) in the east, and southward, (negative) in the west. The residual term, dominated presumably by the convergence of transient eddy vorticity flux, is significant, also consistent with previous analyses (Peng et al. 1997; Peng and Whitaker 1999; Peng and Robinson 2001). A similar vorticity budget is also similar for FCE (Fig. A2b) and TCE (Fig. A2c).

APPENDIX B

Mechanism of SST Propagations

Here, we give a more complete discussion on the heat budget of the surface ocean. First, east of the initial SST anomaly (east of 180°), the ensemble mean SST anomaly shows a rapid eastward expansion in AMIP (Fig. B1a), FCE (Fig. B1b), TCE (Fig. B1c), and less clearly in FXE (Fig. B1d). (Notice that in our AMIP and FXE, surface atmospheric variables and the predicted SST are used to calculate the full heat flux on the ocean.) This eastward propagation is caused by the downstream warming of the ocean by a downward surface heat flux (heat loss to the atmosphere) (Figs. 9a,b). The anomalous heat flux is caused by the warm atmosphere in the downstream, which in turn is warmed by the upstream SST. In FCE, the downstream warming is further enhanced by the positive feedback associated with the

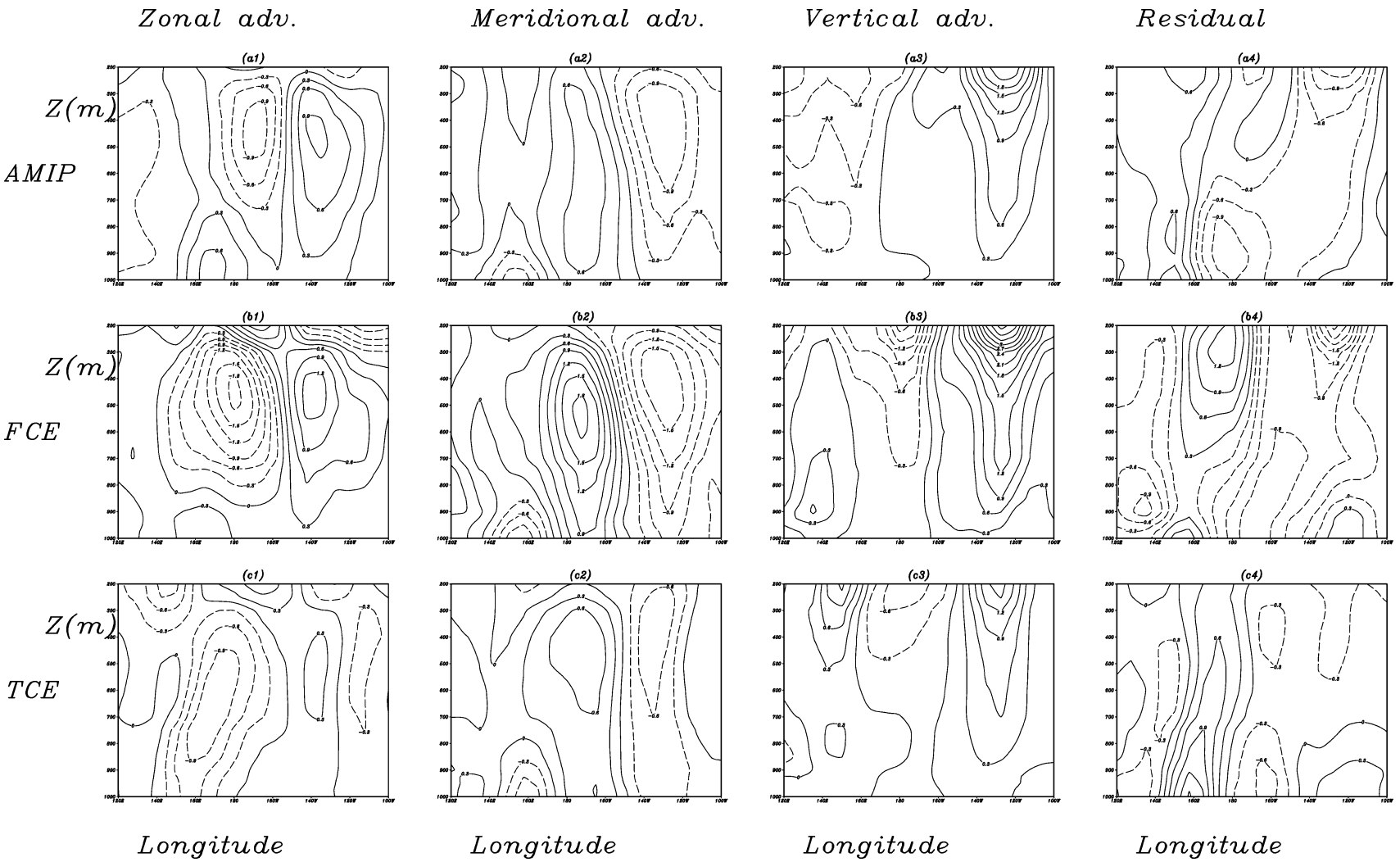

FIG. A1. The anomalous thermodynamic budget on a vertical cross section averaged in the latitude band of 35°–45°N for Dec. (a1) The anomalous zonal temperature advection, (a2) the meridional advection, (a3) the vertical advection, and (a4) the anomalous forcing Q to Eq. (A1) in AMIP. (b) and (c) are the same as (a), but for FCE and TCE, respectively. The contour interval is 0.3 K day^{-1}.

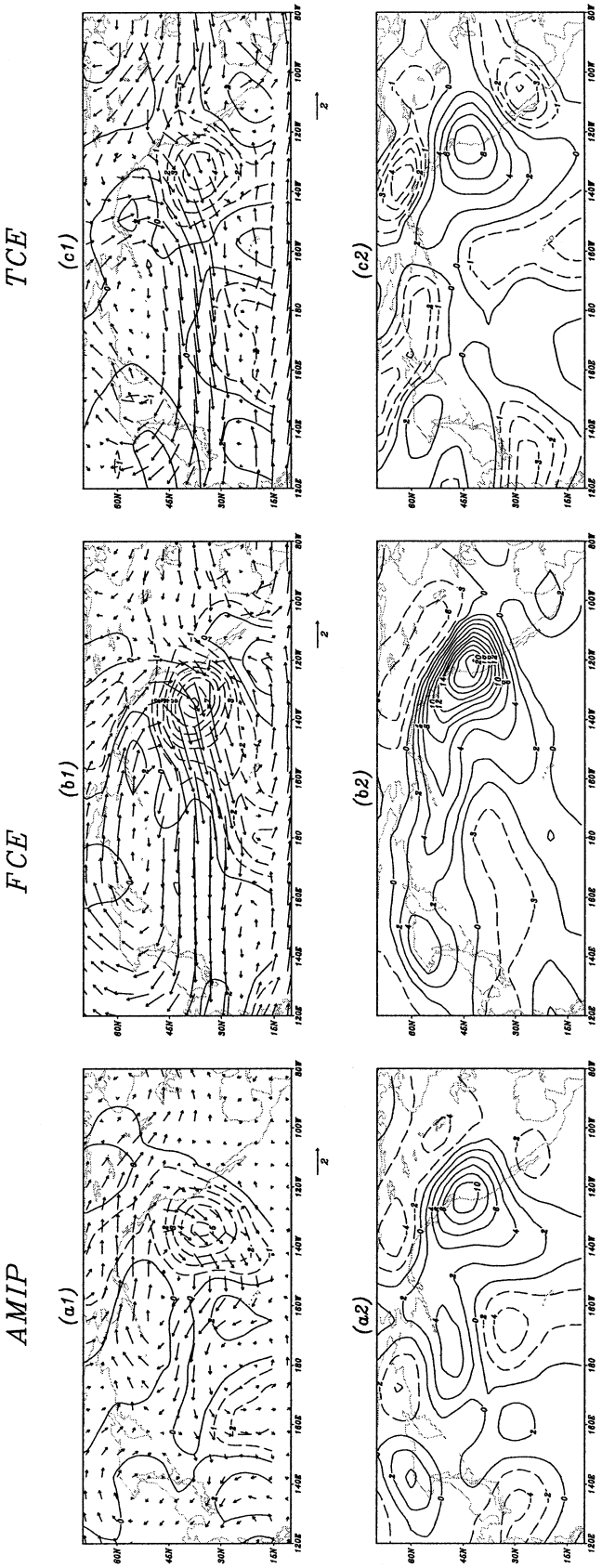

FIG. A2. The 850-hPa anomalous streamfunction tendencies due to horizontal vorticity advection, the divergence term, and the residual term calculated using the monthly data according to Eq. (A2) for (a) AMIP, (b) FCE, and (c) TCE (contour interval 2 $m^2 s^{-2}$). In (c), it is seen that ridge is contributed by the negative vorticity forcing associated with the mean southward flow and the residual vorticity forcing. The former is associated with a mean descending flow that may be induced by the eddy forcing.

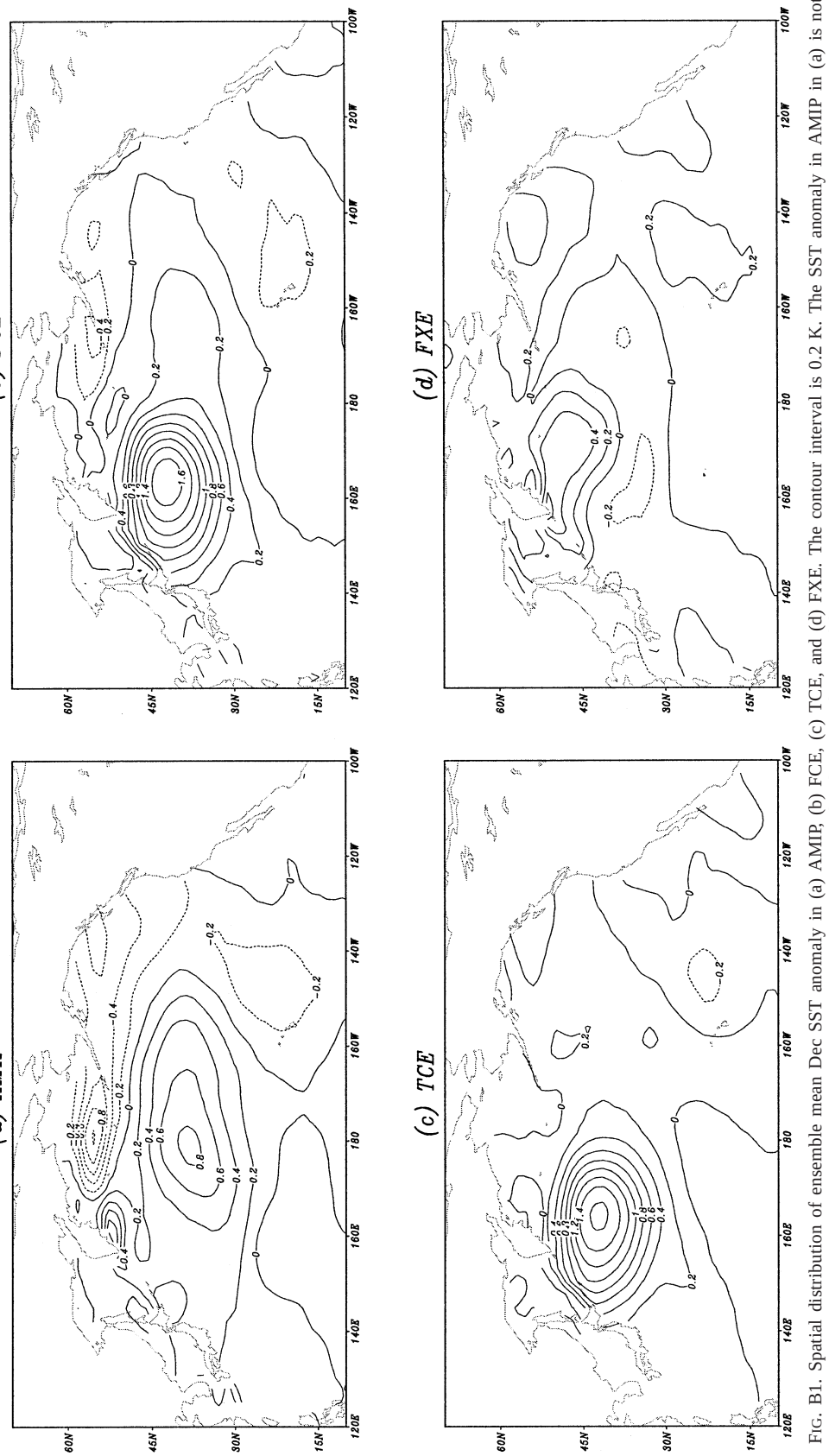

FIG. B1. Spatial distribution of ensemble mean Dec SST anomaly in (a) AMIP, (b) FCE, (c) TCE, and (d) FXE. The contour interval is 0.2 K. The SST anomaly in AMIP in (a) is not seen by the atmosphere model.

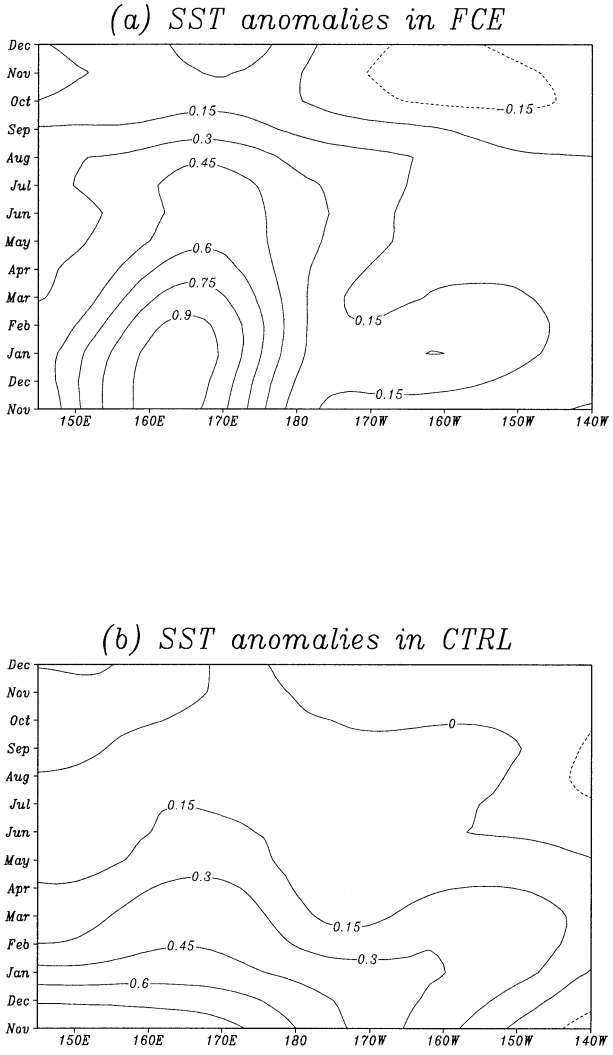

FIG. B2. SST evolution along the latitude band 35°–45°N. (a) Time–longitude plot of the evolution of the ensemble mean SST anomaly in a 14-month integration of the FCE. (b) Lagged regression between the SST averaged in the Kuroshio Extension region and SST anomaly of the following calendar months in the CTRL. Both are normalized by the maximum for comparison. In both cases, the SST show two eastward propagation signals, one fast and one slow.

northward Ekman advection (Fig. 9a). The surface warming stabilizes the upper ocean, reducing convective warming downstream (Figs. 9a,b). This rapid SST propagation occurs at monthly time scales, as seen clearly in the time–longitude plot of the ensemble SST response in FCE (Fig. B2a) and the statistical estimation from the CTRL simulation (Fig. B2b), and is caused mainly by the downstream atmospheric teleconnection as discussed above.

In addition to this rapid eastward propagation, the SST anomaly also shows a slow propagation at interannual time scales locally over the SST anomaly (west of 180°), as also seen clearly in the time–longitude plots of FCE (Fig. B2a) and the CTRL (Fig. B2b). The center of the SST anomaly moved from 160° to 170°E in one year, equal to a mean propagation speed of 3.2 cm s^{-1}. This propagation speed is about half of the speed of the model mean current in this region (about 5 cm s^{-1}). The slow down of the local SST propagation is due to the advection of the anomalous meridional geostrophic current on the mean SST gradient, as discussed in the heat budget in Fig. 9. The mean advection, which is dominated by the mean zonal advection UT'_x, advects the SST anomaly eastward, cooling west and warming east of the maximum SST anomaly. This eastward advection, however, is slowed down by the anomalous meridional current as follows. The perturbation meridional advection can be decomposed into the advection by the anomalous Ekman flow and geostrophic flow as $v'\overline{T}_y = v'_E\overline{T}_y + v'_g\overline{T}_y$. The northward anomalous Ekman flow generates a dominant warming over the SST, while the geostrophic current leads to a westward propagation. The latter term is seen most clearly in TCE in Fig. 9b, in which the anomalous Ekman flow is eliminated and, therefore, $v'\overline{T}_y = v'_g\overline{T}_y$ and shows a warming to the west (cooling to the east) of the maximum SST anomaly. This westward propagation is easy to understand: a deep warm anomaly in the mixed layer is associated with a high pressure anomaly and, in turn, an anticyclonic circulation that is northward west of the maximum SST anomaly. Since the mean SST decreases to the north, the anomalous current warms (cools) the western (eastern) side of the SST anomaly, resulting in a westward propagation. This westward propagation due to $v'_g\overline{T}_y$ is strongest in the midlatitude Kuroshio Extension region because of the strongest mean SST gradient $\overline{T}_y$ there. This mechanism should contribute to a general slow down of the SST anomaly in the midlatitude ocean. The westward propagation due to $v'_g\overline{T}_y$ can also be viewed as a top boundary topographic Rossby wave with a mean temperature gradient equatorward on the boundary.

REFERENCES

Alexander, M. A., C. Deser, and M. S. Timlin, 1999: The reemergence of SST anomalies in the North Pacific Ocean. *J. Climate,* **12,** 2419–2433.

Barsugli, J. J., and D. S. Battisti, 1998: The basic effects of atmosphere–ocean thermal coupling on midlatitude variability. *J. Atmos. Sci.,* **55,** 477–493.

Boville, B. A., and P. Gent, 1998: The NCAR Climate System Model, version one. *J. Climate,* **11,** 1115–1130.

Bretherton, C. S., and D. Battisti, 2000: An interpretation of the results from atmospheric general circulation models forced by the time history of the observed sea surface temperature distribution. *Geophys. Res. Lett.,* **27,** 767–770.

Cajza, A., and C. Frankignoul, 2002: Observed impact of Atlantic SST anomalies on the North Atlantic Oscillation. *J. Climate,* **15,** 606–623.

Deser, C., 2000: On the teleconnectivity of the ''Arctic Oscillation.'' *Geophys. Res. Lett.,* **27,** 779–782.

Ferranti, L., F. Molteni, and T. N. Palmer, 1994: Impact of localized tropical and extratropical SST anomalies in ensembles of seasonal GCM integrations. *Quart. J. Roy. Meteor. Soc.,* **120,** 1613–1645.

Frankignoul, C., 1985: Sea surface temperature anomalies, planetary

waves and air-sea feedback in the middle latitudes. *Rev. Geophys.,* **23,** 357–390.
——, and K. Hasselmann, 1977: Stochastic climate models. II. Application to sea-surface temperature anomalies and thermocline variability. *Tellus,* **29,** 289–305.
——, A. Czaja, and B. L'Heveder, 1998: Air–sea feedback in the North Atlantic and surface boundary conditions for ocean models. *J. Climate,* **11,** 2310–2324.
Hoskins, B. J., and D. J. Karoly, 1981: The steady linear response of a spherical atmosphere to thermal and orographic forcing. *J. Atmos. Sci.,* **38,** 1179–1196.
Jacob, R., 1997: Low frequency variability in a simulated atmosphere ocean system. Ph.D. thesis, University of Wisconsin—Madison, 155 pp.
Kushnir, Y., and N. C. Lau, 1992: The general circulation model response to a North Pacific SST anomaly: Dependence on timescale and pattern polarity. *J. Climate,* **5,** 271–283.
——, and I. Held, 1996: Equilibrium atmospheric response to North Atlantic SST anomalies. *J. Climate,* **9,** 1208–1220.
——, W. A. Robinson, I. Blade, N. M. J. Hall, S. Peng, and R. Sutton, 2002: Atmospheric GCM response to extratropical SST anomalies: Synthesis and evaluation. *J. Climate,* **15,** 2233–2256.
Latif, M., and T. Barnett, 1994: Causes of decadal climate variability over the North Pacific and North America. *Science,* **266,** 634–637.
——, and ——, 1996: Decadal climate variability over the North Pacific and North America: Dynamics and predictability. *J. Climate,* **9,** 2407–2423.
Liu, Z., J. Kutzbach, and L. Wu, 2000: Modeling climatic shift of El Niño variability in the Holocene. *Geophys. Res. Lett.,* **27,** 2265–2268.
——, L. Wu, R. Gallimore, and R. Jacob, 2002: Search for the origins of Pacific decadal climate variability. *Geophys. Res. Lett.,* **29,** 1401, doi:10.1029/2001GL013735.
——, B. Otto-Bliesner, J. Kutzbach, L. Li, and C. Shields, 2003: Coupled climate simulations of the evolution of global monsoons in the Holocene. *J. Climate,* **16,** 2472–2490.
Otto-Bliesner, B. L., and E. C. Brady, 2001: Tropical Pacific variability in the NCAR Climate System Model. *J. Climate,* **14,** 3587–3607.
Palmer, T., and Z. Sun, 1985: A modeling and observational study of the relationship between sea-surface temperature in the northwest Atlantic and the atmospheric general circulation. *Quart. J. Roy. Meteor. Soc.,* **111,** 947–975.
Peng, S., and J. S. Whitaker, 1999: Mechanisms determining the atmospheric response to midlatitude SST anomalies. *J. Climate,* **12,** 1393–1408.
——, and W. A. Robinson, 2001: Relationships between atmospheric internal variability and the responses to an extratropical SST anomaly. *J. Climate,* **14,** 2943–2959.
——, A. Mysak, H. Ritchie, J. Derome, and B. Dugas, 1995: The difference between early and middle winter atmospheric response to sea surface temperature anomalies in the northwest Atlantic. *J. Climate,* **8,** 137–157.
——, W. A. Robinson, and M. P. Hoerling, 1997: The modeled atmospheric resonse to midlatitude SST anomalies and its dependence on background circulation states. *J. Climate,* **10,** 971–987.
Pitcher, E. J., M. L. Blackmon, G. T. Bates, and S. Munoz, 1988: The effect of North Pacific sea surface temperature anomalies on the January climate of a general circulation model. *J. Atmos. Sci.,* **45,** 172–188.
Saravanan, R., and P. Chang, 1999: Oceanic mixed layer feedback and tropical Atlantic. *Geophys. Res. Lett.,* **26,** 3629–3632.
Sutton, R., and P. P. Mathieu, 2002: Response of the atmosphere–ocean mixed layer system to anomalous ocean heat flux convergence. *Quart. J. Roy. Meteor. Soc.,* **128,** 1259–1275.
Thompson, D. J. W., and J. M. Wallace, 1998: The Arctic oscillation signature in wintertime geopotential height and temperature fields. *Geophys. Res. Lett.,* **25,** 1297–1300.
Toth, Z., and E. Kalnay, 1997: Ensemble forecasting at NMC and the breeding method. *Mon. Wea. Rev.,* **125,** 3297–3319.
Wu, L., and Z. Liu, 2003: Decadal variability in North Pacific: The eastern North Pacific mode. *J. Climate,* **16,** 3111–3131.
——, ——, R. Gallimore, R. Jacob, D. Lee, and Y. Zhong, 2003: A coupled modeling study of Pacific decadal variability: The tropical mode and the North Pacific mode. *J. Climate,* **16,** 1101–1120.
Yulaeva, E., N. Schneider, D. Pierce, and T. Barnett, 2001: Modeling of North Pacific climate variability forced by oceanic heat flux anomalies. *J. Climate,* **14,** 4027–4046.